Cellular/Molecular

Transferrin Receptor Is Necessary for Proper Oligodendrocyte Iron Homeostasis and Development

Veronica T. Cheli,* Diara A. Santiago González,* Rensheng Wan,* Shaina L. Rosenblum, Giancarlo E. Denaroso, Christina G. Angeliu, Zachary Smith, Congying Wang, and Pablo M. Paez
Institute for Myelin and Glia Exploration, Department of Pharmacology and Toxicology, Jacobs School of Medicine and Biomedical Sciences, State University of New York, University at Buffalo, Buffalo, New York 14203

To test the hypothesis that the transferrin (Tf) cycle has unique importance for oligodendrocyte development and function, we disrupted the expression of the Tf receptor (Tfr) gene in oligodendrocyte progenitor cells (OPCs) on mice of either sex using the *Cre/lox* system. This ablation results in the elimination of iron incorporation via the Tf cycle but leaves other Tf functions intact. Mice lacking Tfr, specifically in NG2 or Sox10-positive OPCs, developed a hypomyelination phenotype. Both OPC differentiation and myelination were affected, and Tfr deletion resulted in impaired OPC iron absorption. Specifically, the brains of Tfr cKO animals presented a reduction in the quantity of myelinated axons, as well as fewer mature oligodendrocytes. In contrast, the ablation of Tfr in adult mice affected neither mature oligodendrocytes nor myelin synthesis. RNA-seq analysis performed in Tfr cKO OPCs revealed misregulated genes involved in OPC maturation, myelination, and mitochondrial activity. Tfr deletion in cortical OPCs also disrupted the activity of the mTORC1 signaling pathway, epigenetic mechanisms critical for gene transcription and the expression of structural mitochondrial genes. RNA-seq studies were additionally conducted in OPCs in which iron storage was disrupted by deleting the ferritin heavy chain. These OPCs display abnormal regulation of genes associated with iron transport, antioxidant activity, and mitochondrial activity. Thus, our results indicate that the Tf cycle is central for iron homeostasis in OPCs during postnatal development and suggest that both iron uptake via Tfr and iron storage in ferritin are critical for energy production, mitochondrial activity, and maturation of postnatal OPCs.

Key words: **ferritin; iron; myelination; oligodendrocyte; transferrin; transferrin receptor**

Significance Statement

By knocking-out transferrin receptor (Tfr) specifically in oligodendrocyte progenitor cells (OPCs), we have established that iron incorporation via the Tf cycle is key for OPC iron homeostasis and for the normal function of these cells during the postnatal development of the CNS. Moreover, RNA-seq analysis indicated that both Tfr iron uptake and ferritin iron storage are critical for proper OPC mitochondrial activity, energy production, and maturation.

Introduction

Throughout the postnatal development of the brain, iron is first detected in oligodendrocyte progenitor cells (OPCs) proximal to blood vessels (Burdo et al., 1999) and then in premyelinating and mature oligodendrocytes localized in areas of active myelination (Connor and Menzies, 1996). This observation denotes a functional relationship between oligodendrocyte iron uptake and myelin production (Taylor and Morgan, 1990). OPCs, as well as mature myelinating oligodendrocytes, possess the highest intracellular concentration of iron in any CNS cell type (Reinert et al., 2019). Iron is essential for oligodendrocyte function: oligodendrocytes require iron as a cofactor for several enzymes involved in cholesterol and phospholipid production, as well as for normal mitochondria activity and ATP synthesis (Stephenson et al., 2014). Consequently, iron deficiency during early postnatal development reduces myelin synthesis and delays OPC development (Beard et al., 2003; Ortiz et al., 2004).

Circulating plasma iron binds to transferrin (Tf), which solubilizes the ferric iron and attenuates its reactivity. Diferric Tf interacts with cell-surface Tf receptor (Tfr) to undergo receptor-mediated endocytosis into specialized endosomes (Roetto et al., 2002). Endosomal acidification leads to iron release, and iron is

Received July 15, 2022; revised Mar. 15, 2023; accepted Mar. 21, 2023.
Author contributions: V.T.C. and P.M.P. designed research; V.T.C., D.A.S.G., R.W., S.L.R., G.E.D., C.G.A., Z.S., C.W., and P.M.P. performed research; V.T.C., D.A.S.G., R.W., S.L.R., G.E.D., C.G.A., Z.S., C.W., and P.M.P. analyzed data; V.T.C., D.A.S.G., R.W., G.E.D., and P.M.P. wrote the first draft of the paper; V.T.C., G.E.D., C.G.A., and P.M.P. edited the paper; V.T.C. and P.M.P. wrote the paper.
This work was supported by National Institute of Neurological Disorders and Stroke Award 2R01NS078041 and the Legacy of Angels Foundation.
*V.T.C., D.A.S.G., and R.W. contributed equally to this work.
The authors declare no competing financial interests.
Correspondence should be addressed to Pablo M. Paez at ppaez@buffalo.edu.
https://doi.org/10.1523/JNEUROSCI.1383-22.2023

subsequentially transported out of the endosome through the activity of divalent metal transporter 1 (DMT1), a transmembrane iron transporter (Cheli et al., 2018). Tf and Tfr then return to the cell surface for reuse, completing a highly efficient cycle. In the brain, Tf is synthesized by immature oligodendrocytes and epithelial cells of the choroid plexus (Bloch et al., 1985; Espinosa de los Monteros et al., 1994). It was established that increased levels of Tf in the CNS of rodents significantly increase myelin production (Escobar-Cabrera et al., 1997; Saleh et al., 2003), stimulates OPC differentiation (Paez et al., 2004, 2005, 2006), and promotes remyelination in demyelinating models (Adamo et al., 2006; Guardia-Clausi et al., 2012).

Although the Tf cycle is assumed to be the general mechanism for oligodendrocyte iron uptake, this presumption has not been validated experimentally. Previous studies have shown that Tfr is present in endothelial cells of brain capillaries and neurons, but not in OPCs and/or oligodendrocytes (Roberts et al., 1993). However, some works indicate that Tfr is expressed by OPCs but downregulated in myelinating oligodendrocytes (Li et al., 2013; Y. Zhang et al., 2014). Therefore, to test the hypothesis that the Tf cycle is essential for oligodendrocyte maturation and function, we have deleted the Tfr in oligodendroglial cells at different developmental time points. We found that Tfr ablation in early OPCs results in oligodendrocyte iron deficiency and hypomyelination. In contrast, Tfr deletion in young myelinating oligodendrocytes does not affect myelin synthesis or maintenance. Furthermore, RNA-seq analysis in acute isolated cortical OPCs indicates that Tfr expression is central for normal mitochondrial activity, energy production, and maturation of postnatal OPCs. Transcriptomic studies were also performed in OPCs in which the ferritin heavy subunit (Fth) was deleted. Fth is the main intracellular iron-storage protein (Y. Zhang et al., 2010) and is essential for OPC maturation (Wan et al., 2020). Suggesting that Fth is central for proper OPC iron homeostasis and function, gene sets associated with iron metabolism, antioxidant activity, and myelination were significantly misregulated in Fth cKO OPCs.

Materials and Methods

Transgenic mice. All animals used in the present study were housed in the University at Buffalo Division of Laboratory Animal Medicine vivarium. Procedures were approved by University at Buffalo's Animal Care and Use Committee and conducted in accordance with the guidelines in *Guide for the care and use of laboratory animals* from the National Institutes of Health. The following transgenic mice were obtained from The Jackson Laboratory: floxed ferritin heavy chain (Fth) (Darshan et al., 2009; JAX stock #018063), floxed transferrin receptor 1 (Tfr) (JAX stock #028177), *Cre* reporter (Ai9 (RCL-tdT) (JAX stock #007909), Sox10*Cre*ER^{T2} (Matsuoka et al., 2005; JAX stock #025807), and NG2*Cre*ER^{T2} (Zhu et al., 2011; JAX stock #008538). Experimental animals were generated by crossing the heterozygous floxed lines with the hemizygous Sox10*Cre*ER^{T2} or NG2*Cre*ER^{T2} transgenic mice. In all the experiments presented in this work, mice of either sex were used.

Mice treatments. To delete Tfr in OPCs, *Cre* activity was induced by tamoxifen starting at postnatal day 2 (P2). P2 Sox10-Tfr^{KO} (Tfr$^{f/f}$, Sox10*Cre*ER$^{Cre/-}$) or NG2-Tfr^{KO} (Tfr$^{f/f}$, NG2*Cre*ER$^{Cre/-}$) and control (*Cre*-negative) littermates (Tfr$^{f/f}$, Sox10*Cre*ER$^{-/-}$ or NG2*Cre*ER$^{-/-}$) were intraperitoneally injected once a day for 5 consecutive days with 25 mg/kg tamoxifen (Sigma-Aldrich), and brain tissue was collected at P15 and P30. Furthermore, P30 and P60 Sox10-Tfr^{KO} and control littermates were injected intraperitoneally once a day for 5 consecutive days with 100 mg/kg tamoxifen, and brain tissue was collected at P60 and P90, respectively. To delete Fth in OPCs, P2 Sox10-Fth^{KO} (Fth$^{f/f}$, Sox10*Cre*ER$^{Cre/-}$) and control (*Cre*-negative) littermates (Fth$^{f/f}$, Sox10*Cre*ER$^{-/-}$) were intraperitoneally injected once a day for 5 consecutive days with 25 mg/kg tamoxifen, and cortical OPCs were collected at P15.

Primary cultures of cortical OPCs. Primary cultures of cortical OPCs were prepared as described by Cheli et al. (2015). First, cerebral hemispheres from 1-day-old mice were mechanically dissociated and were plated on poly-D-lysine-coated flasks in DMEM/F12 (1:1 v/v) (Invitrogen), supplemented with 10% FBS (Invitrogen). After 4 h, the medium was changed and the cells were grown in DMEM/F12 supplemented with insulin (5 μg/ml), apotransferrin (50 μg/ml), sodium selenite (30 nM), D-biotin (10 mM), and 10% FBS (Invitrogen). Two-thirds of the culture media was changed every 3 d. OPCs were purified from the mixed glial culture after 14 d by a differential shaking and adhesion procedure and allowed to grow on poly-D-lysine-coated coverslips in DMEM/F12 supplemented with insulin (5 μg/ml), apotransferrin (50 μg/ml), sodium selenite (30 nM), 0.1% BSA, progesterone (0.06 ng/ml), and putrescine (16 μg/ml) (Sigma). OPCs were kept in mitogens, PDGF and bFGF (20 ng/ml) (Peprotech), for 2 d and then induced to differentiate by mitogen withdrawal and T3 (15 nM). To induce *Cre*-mediated recombination, control and Sox10-Tfr^{KO} OPCs were treated with 4-OH-tamoxifen (1.5 μM) for 3 consecutive days starting 1 d after plating. Since litter size significantly affects pup development, litters with <5 or >10 pups were not used.

Immunocytochemistry. Cells were immunostained following the protocol outlined by Cheli et al. (2016). Images were obtained using an Olympus IX83-DSU microscope, and quantitative analysis of the results was done by counting the antigen-positive and Olig2-positive cells in 20 randomly selected fields per coverslip, which resulted in counts of >2000 cells. Four coverslips per experimental condition were analyzed, and data represent pooled results from at least three independent cultures. Cell counting was completed semiautomatically by MetaMorph software (Molecular Devices). Primary antibodies area as follows: CC1 (mouse; 1:300; Calbiochem), CNP (rabbit; 1:1000; Neo-Markes), Ki67 (mouse; 1:200; BD Bio-sciences), MOG (mouse; 1:200; Millipore), NG2 (rabbit; 1:400; Millipore), Olig1 (mouse; 1:400; Chemi-Con), Olig2 (mouse and rabbit; 1:500; Millipore), and Tfr (mouse; 1:250; Fisher Scientific).

Colorimetric iron assay. The Quantichrom iron assay kit (BioAssay Systems) was used to measure total cellular iron. Briefly, 50 μl of samples containing 1×10^6 cells were mixed with 200 μl Quantichrom working reagent in a 96-well plate and incubated at room temperature for 40 min. The optical density (OD) at 590 nm was measured by a microplate reader. The OD against standard iron concentrations was plotted by subtracting blank (water) OD from the standard OD values, and the slope of the data plot then determined using linear regression. The total protein concentration was estimated using the Pierce BCA Protein Assay Kit (Fisher Scientific).

Western blot. Protein samples were extracted using lysis buffer as described by Santiago González et al. (2017); 20 µg of proteins was separated with NuPAGE Novex 4%-12% Bis-Tris Protein Gels (Invitrogen) and electroblotted onto PDVF membranes. Membranes were blocked overnight at 4°C with 5% nonfat milk, 0.1% Tween-20 in PBS. Primary antibodies were diluted in a blocking solution and membranes incubated 3 h at room temperature with agitation. Protein bands were detected using the GE Healthcare ECL kit (GE Healthcare) with HRP-conjugated secondary antibodies (GE Healthcare) and scanned with a C-Digit Bot Scanner (LI-COR). Protein bands were quantified using the Image Studio Software (LI-COR). Primary antibodies are as follows: β-actin (mouse; 1:10,000; Sigma-Aldrich), CNP (1:1000; Neo-Markes), MBP (mouse; 1:1000; Covance), PLP (rat; 1:500, AA3-PLP/DM20), P84 (mouse; 1:10,000; GeneTex), Tfr (mouse; 1:2500; Fisher Scientific), and α-tubulin (mouse; 1:10 000; Proteintech).

RT-PCR. Total RNA was isolated using Trizol (Invitrogen). RNA content was estimated by measuring the absorbance at 260 nm, and the purity was assessed by measuring the ratio of absorbance: 260/280 nm. PCR primers were designed based on published sequences. First-strand cDNA was prepared from 1 µg of total RNA using SuperScriptTM III RNase H-reverse transcriptase (Invitrogen) and 1 µg of oligo(dT). The mRNA samples were denaturized at 65°C for 5 min. Reverse transcription was performed at 50°C for 55 min and was stopped by heating the samples at

85°C for 5 min. The cDNA was amplified using PCR Platinum Supermix (Invitrogen). PCR conditions were as follows: 94°C for 2 min, 40 cycles of 94°C for 30 s, 58°C for 30 s followed by 72°C for 2 min. After 40 cycles, samples were incubated at 72°C for 5 min. The PCR products were visualized on a SYBR Safe-stained agarose gel, and the bands digitized using a Gel Doc EZ System (Bio-Rad).

qPCR. Total RNA was extracted and purified from NG2-positive OPCs as described in RNA-Seq. Briefly, 500 µg of RNA was reverse-transcribed using PrimeScript first strand cDNA Synthesis Kit (Takara). qPCR was performed using a CFX96 Touch Real-Time PCR Detection Systems (Bio-Rad) and SYBR Green PCR Master Mix (Applied Biosystems). qPCR conditions were as follows: polymerase activation 95°C, 10 min, followed by 40 cycles: denaturation at 95°C, 15 s; primer annealing/elongation at 60°C, 60 s. Primer specificity was analyzed adding a melting curve for each reaction. Quantification of PCR products was conducted using the Pfaffl method. Quantities of mRNA were normalized to the housekeeping genes GAPDH and TBP. The following primers were used: Tfr forward: AGCAAAGTCTGGCGAGATGA, reverse: ATGCCACATAACCCTCGGGA (Efficiency 1.968); GAPDH forward: GTGAACCACGAGAAATATGACAAC, reverse: AGTGATGGCATGG ACTGTG (Efficiency 1.933), and TBP forward: CCTTGTACCCTT CACCAATGAC, reverse: ACAGCCAAGATTCACGGTAGA (Efficiency 1.959).

RNA-seq. Oligodendrocytes were isolated from P15 mouse brains using the magnetic cell sorting technique. The corpus callosum and the adjacent cortical area were dissected, and single-cell suspensions were prepared as described by Zamora et al. (2020). Oligodendrocytes were magnetically labeled using the anti-AN2 Microbeads kit and separated using a LS column according to manufacturer's instructions (Miltenyi Biotec). Total RNA was extracted using the RNeasy Plus Mini Kit (QIAGEN). Samples containing 1 µg of total RNA with RNA quality number >8.0 were used for RNA library preparation using the Illumina TruSeq Stranded Total RNA kit with Ribo-Zero. Two replicates of 4 pooled animals (2 males and 2 females) for each experimental condition were sequenced. Quality controls were performed for all the RNA libraries, including Qubit and Fragments Analyzer. Only RNA libraries with concentrations >10 ng/µl and no RNA fragments <200 bp were used for analysis. RNA-seq was performed using the Illumina Nova Seq 6000 system which provided a minimum of 20-25 million reads per sample. RNA-seq reads were aligned to the Mus musculus genome (mm10) (UC, Santa Cruz, Genome Browser) using STAR (Ultrafast Universal RNA-seq Aligner Software) (Dobin et al., 2013), quantified using the FeatureCount software (Liao et al., 2014) and the quality control was performed using Multi QC (www.usegalaxy.org). Normalization and differential gene expression were done using the DESeq2 package (Love et al., 2014). Clustering of genes for the final heatmap of differentially expressed genes were performed via R Package ClusterProfiler (Wu et al., 2021). Several databases were used for gene ontology and enrichment analysis, including Gene Ontology (www.geneontology.org), DAVID (www.david.ncifcrf.gov), REACTOME (www.reactome.org), and gene set enrichment analysis (GSEA; www.gsea-msigdb.org).

Immunohistochemistry. Animals were perfused with 4% of PFA in PBS via the left ventricle and the brains were postfixed overnight in the same fixative solution at 4°C. Coronal brain slices of 50 µm thick were obtained using a vibratome (Leica Biosystems, VT1000-S). Free-floating vibratome sections were incubated in a blocking solution (2% normal goat serum and 1% Triton X-100 in PBS) for 2 h at room temperature and then incubated with the primary antibody overnight at 4°C. Sections were then rinsed in PBS and incubated with Cy3- or Cy5-conjugated secondary antibodies (1:400; Jackson ImmunoResearch Laboratories) for 2 h at room temperature. After washing, the sections were mounted on to Superfrost Plus slides (Fisher) using coverslips and mounting medium (Aquamount; Fisher Scientific). The staining intensity for myelin proteins and the number of positive cells was assessed in the central area of the corpus callosum, between the midline and below the apex of the cingulum (0.6 mm^2), in the motor and cingulate cortex, including M1, M2, Cg1, Cg2 (0.6 mm^2) (Franklin and Paxinos, 2008, their Fig. 24) and in the dorsal/caudal striatum, immediately underneath the corpus callosum (0.6 mm^2). The integrated fluorescence intensity was calculated as the product of the area and mean pixel intensity using MetaMorph software (Molecular Devices). For all experiments involving quantification of positive cells and fluorescent intensity in tissue sections, data represent pooled results from at least six brains per experimental group. Fifteen slices per brain (50 μm each) were used, and quantification was completed blind to the genotype of the sample. Primary antibodies: caspase-3 (mouse; 1:200; Cell Signaling), CC1 (mouse; 1:300; Calbiochem), Ki67 (rabbit; 1:250; Abcam), Ki67 (mouse; 1:250; BD Biosciences), MBP (mouse; 1:1000; Covance), Olig2 (mouse and rabbit; 1:500; Millipore), PLP (rat; 1:250, AA3-PLP/DM20), Sox2 (rabbit; 1:200; Millipore), and Tfr (mouse; 1:500; Fisher Scientific).

Black Gold II myelin staining. Black Gold II staining was performed as described in Cheli et al. (2016). PFA-fixed brain sections of 50 μm were mounted onto Superfrost Plus slide (Fisher Scientific). Coronal brain slices were initially air-dried and then rehydrated and transferred to a lukewarm 0.3% Black Gold II solution (Millipore). After color development (~10 min), the slides were rinsed with a 1% sodium thiosulfate solution at 60°C, dehydrated and mounted with Permount. The integrated staining intensity was assessed by MetaMorph software (Molecular Devices). The staining intensity in Sox10-Tfr^{KO} mice was determined as a percentage of that in control mice. Fifteen slices per brain (50 μm each) were used, and data represent pooled results from at least four brains per experimental group.

Perls' histochemistry. Enhanced Perls' histochemistry was performed as described previously by Cheli et al. (2018). Briefly, 20 µm coronal brain sections were incubated with 1% H_2O_2 in methanol for 15 min and then with 2% potassium ferrocyanide (pH 1.0) overnight (Iron Stain Kit, Sigma-Aldrich). The reaction was enhanced for 30 min with 0.025% 3,3'-diaminobenzidine-4Hl, 0.05% H_2O_2 and 0.005% $CoCl_2$ in 0.1 M PB. Finally, sections were dehydrated and mounted with Permount. The number of positive oligodendrocytes and the integrated staining intensity per cell was assessed by MetaMorph (Molecular Devices) in the central area of the corpus callosum, between the midline and below the apex of the cingulum (0.6 mm^2) and in the motor and cingulate cortex, including M1, M2, Cg1, Cg2 (0.6 mm^2) (Franklin and Paxinos, 2008, their Fig. 24). Twelve slices per brain (20 μm each) were used, and data represent pooled results from at least four brains per experimental group.

Electron microscopy. Mice were perfused transcardially with 3% PFA and 1% glutaraldehyde, and the brains were removed. The body of the corpus callosum at the anterior-dorsal level of the hippocampus was dissected and resin embedded. Thin sections were stained with uranyl acetate and lead citrate and photographed with a FEI Tecnai F20 transmission electron microscope as previously described (Cheli et al., 2016). For *g*-ratio measurements, at least 200 fibers per animal were analyzed. The percentage of myelinated axons was determined in 20 randomly selected fields per sample, which resulted in counts of >1000 axons. The *g*-ratio and the percentage of myelinated axons were determined semiautomatically and blind to the genotype of the sample using MetaMorph (Molecular Devices). For all experimental conditions, data represent pooled results from at least 4 mice.

Statistical analysis. All datasets were tested for normal distribution using the Kolmogorov–Smirnov test. Single between-group comparisons were made by the unpaired *t* test (Student's *t* test), using a CI of 95%. Multiple comparisons were investigated by one-way ANOVA followed by Bonferroni's multiple comparison test to detect pairwise between-group differences. For the analysis of *g*-ratio scatter plots, simple linear regression with a CI of 95% was used. All statistical tests were performed in GraphPad Prism (GraphPad Software). A fixed value of $p < 0.05$ for two-tailed test was the criterion for reliable differences between groups. Data are presented as mean ± SEM. To minimize bias, all experimental quantifications were completed blinded to the sample genotype. Based on previous studies, power calculations and the fact that all comparisons were made between mice with the same genetic background, at least 4 mice for each genotype were compared for all the morphologic and biochemical endpoints.

Results

Conditional deletion of Tfr in cortical OPCs

A conditional KO mouse for the Tfr in oligodendrocytes was generated by cross-breeding the floxed mutant Tfr mouse

(Gunshin et al., 2005; Carlson et al., 2009) with the Sox10-*Cre*ER transgenic line (Zhu et al., 2011). Initially, OPCs were isolated from the cortex of P1 Tfr KO mice (Sox10-Tfr^{KO}; Tfr$^{f/f}$, Sox10-*Cre*ER$^{Cre/-}$) and control (*Cre* negative) littermates (Control; Tfr$^{f/f}$, Sox10-*Cre*ER$^{-/-}$), and *Cre*-mediated recombination was induced *in vitro* by 4-OH-tamoxifen. RT-PCR, qPCR, Western blot, and immunocytochemical experiments for Tfr revealed high recombination efficiency and decreased Tfr levels in Sox10-Tfr^{KO} OPCs (Fig. 1*A–D*). Iron incorporation was measured using a colorimetric iron assay; compared with controls, Sox10-Tfr^{KO} OPCs showed a ~ 50% decrease in iron content, which correlates well with the decreased expression of Tfr in these cells (Fig. 1*E*). Additionally, the expression of myelin protein, such as CNP and MOG along with the number of mature oligodendrocytes (Olig2/CC1 double-positive cells), was significantly decreased in Sox10-Tfr^{KO} cultures (Fig. 1*F*,*G*). The mitotic marker Ki67 was combined with Olig2 to assess OPC proliferation, and the proportion of OPCs was estimated by analyzing the colocalization of Olig2 with Olig1 and NG2 (Meijer et al., 2012). The number of proliferating Sox10-Tfr^{KO} cells (Olig2/Ki67 double-positive cells) was normal; however, the percentage of immature Olig2/NG2 and Olig2/Olig1 double-positive OPCs was increased relative to control levels (Fig. 1*F*,*G*). Oligodendrocyte morphology was also evaluated following the procedure described by Sperber and McMorris (2001). Individual MOG-positive cells were scored according to their morphologic complexity in four different categories based on the length and number of primary processes, the relative development of secondary and tertiary processes, and the overall size of the cell (Fig. 1*H*). We observed a significant reduction in the morphologic complexity of individual MOG-positive cells in Sox10-Tfr^{KO} cultures (Fig. 1*H*). Specifically, >50% of Sox10-Tfr^{KO} OPCs were classified in the low category (Fig. 1*H*). Overall, these results suggest that Tfr is important for iron incorporation in OPCs and their maturation *in vitro*.

Postnatal deletion of Tfr in the oligodendrocyte lineage

To knock out Tfr in Sox10-positive OPCs during postnatal brain development, *Cre* activity was induced at P2 by intraperitoneal injection of tamoxifen. Sox10-Tfr^{KO} and control littermates were injected once a day for 5 consecutive days with tamoxifen, and brain tissues were collected at P15 and P30 (Fig. 2*A*). *Cre* recombination was evaluated at P15 by RT-PCR and qPCR performed in NG2-positive OPCs isolated from dissociated brain cortices of tamoxifen-treated Sox10-Tfr^{KO} mice (Fig. 2*B*,*C*). The presence of the expected truncated Tfr mRNA in RT-PCR experiments and a significant (~70%) reduction in Tfr mRNA by qPCR indicate a high *Cre* recombination efficacy in our mouse model (Fig. 2*B*,*C*). Cell specificity was evaluated by crossing the Sox10*Cre*ER^{T2} mouse with the *Cre* reporter line Ai9(RCL-tdT). Figure 2*D* shows the expression of the *Cre* reporter fluorescent protein tdTomato in cortical and callosal oligodendrocytes at P15. In this mouse line, we found that five tamoxifen injections starting at P2 induce tdTomato expression in ~95% of cortical and callosal Olig2-positive cells (Fig. 2*D*). Additionally, Tfr expression was measured in oligodendrocytes at P15 by analyzing Tfr fluorescence intensity in the soma of Olig2-positive cells. In agreement with our qPCR results from acute isolated OPCs, Tfr expression was reduced in average 75% in all cortical and callosal Olig2-positive cells (Fig. 2*E*).

Immunohistochemical experiments were first performed to analyze myelin protein synthesis in the brain. At P15, Sox10-Tfr^{KO} mice displayed an average 50% reduction in PLP and MBP immunofluorescence in the corpus callosum and cortex (Fig. 2*F*, *G*). Similar reductions in PLP and MBP levels were found in the same brain areas at P30 (Fig. 2*F*,*G*). Furthermore, tissue was collected from the cortex and cerebellum of control and Sox10-Tfr^{KO} animals for Western blots of myelin proteins (Fig. 2*H*). In agreement with the immunohistochemistry results, the expression levels of MBP, CNP, and PLP were decreased in Sox10-Tfr^{KO} mice at both P15 and P30 (Fig. 2*H*). These results were corroborated using the Black Gold II myelin staining method which labels total myelin lipids. This technique stains large, myelinated tracts dark red-brown, while the individual myelinated fibers appear black (Fig. 3*C*). Sox10-Tfr^{KO} mice displayed an important reduction in the density of myelinated fibers in the corpus callosum and cortex at P15 and P30 (Fig. 3*C*,*D*). Brain tissue from the same animals was used to measure total iron stored in oligodendrocytes. Enhanced Perls' histochemistry was performed in control and Sox10-Tfr^{KO} animals, and the density and staining intensity of positive oligodendrocytes were quantified in the corpus callosum and cortex (Fig. 3*A*,*B*). Suggesting that Tfr-deficient cells do not uptake iron normally, the number of iron-positive oligodendrocytes as well as the intensity of the staining in individual cells were found to be significantly reduced in Sox10-Tfr^{KO} brains (Fig. 3*A*,*B*).

To study the role of Tfr in premyelinating and myelinating oligodendrocytes, Sox10-Tfr^{KO} mice were injected with tamoxifen at P30 and P60, and immunohistochemical analysis for myelin proteins was conducted at P60 and P90, respectively (Fig. 4*A*). Suggesting that the hypomyelination found at P15 and P30 persists after the peak of myelination, the corpus callosum and cortex of P60 Sox10-Tfr^{KO} mice injected with tamoxifen at P30 displayed a significant reduction in PLP and MBP immunostaining (Fig. 4*B*,*C*). Additionally, the levels of MBP, CNP, and PLP in the cortex and cerebellum of P60 Sox10-Tfr^{KO} mice were found to be reduced by Western blot (Fig. 4*D*). In contrast, P90 Sox10-Tfr^{KO} mice injected with tamoxifen at P60 showed similar PLP and MBP expression than control animals (Fig. 4*B*,*C*). Western blot experiments showed similar results, except for a small (~10%) reduction in MBP and CNP in the cerebellum of Sox10-Tfr^{KO} mice at P90 (Fig. 4*D*).

The myelination of the Sox10-Tfr^{KO} brain was also evaluated by electron microscopy. The percentage of myelinated axons and the *g*-ratio of myelinated fibers were analyzed in the body of the corpus callosum at P15 and P30. Sox10-Tfr^{KO} animals exhibited a significant decrease in the percentage of myelinated axons in combination with an increase in the mean *g*-ratio of myelinated fibers at both P15 and P30 (Fig. 5*A–E*). In line with the immunohistochemical results, significant changes between genotypes were found at P15 and P30, but not at P90 (Fig. 5*A–C*). Sox10-Tfr^{KO} mice injected with tamoxifen at P60 and analyzed at P90 displayed no changes in the percentage of myelinated axons and presented small variations in the mean *g*-ratio of myelinated fibers (Fig. 5*A*,*B*,*C*,*E*). Importantly, Sox10-Tfr^{KO} animals exhibited a decrease in the diameter of myelinated axons at P15 but presented an increase at P30 (Fig. 5*D*), suggesting a delay in the myelination process. In summary, these data indicate that oligodendrocytes lacking the Tfr are myelinating fewer axons and are making thinner internodes.

The transcription factor Olig2, which is localized to the oligodendrocyte nucleus at all developmental stages (Meijer et al., 2012), as well as the somatic marker CC1, which is restricted to myelinating oligodendrocytes (Bin et al., 2016), were used to measure total and mature oligodendrocytes, respectively. At P15 and P30, Sox10-Tfr^{KO} animals exhibited a reduction in the total

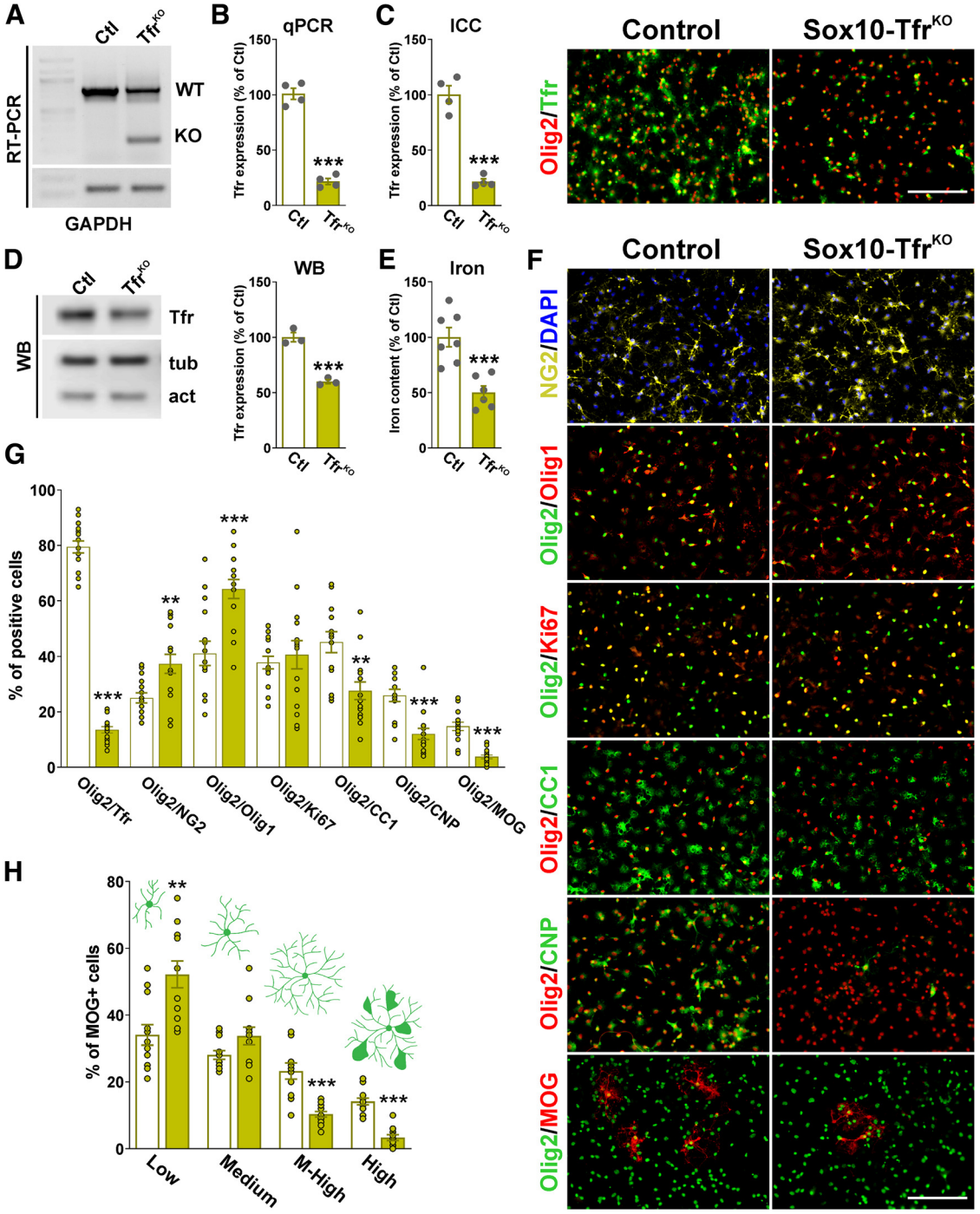

Figure 1. Tfr KO blocks OPC maturation *in vitro*. ***A***, Representative RT-PCR for Tfr in control and Sox10-Tfr^{KO} OPCs performed after 3 d of 4-OH-tamoxifen treatment. GAPDH was used as internal standard. ***B***, qPCR experiments for Tfr were performed in OPCs after 3 d of 4-OH-tamoxifen treatment. Four independent samples per condition were analyzed, and Tfr mRNA was normalized to GAPDH and TBP. Each dot represents the mean of one independent sample. ***C***, Tfr expression was analyzed by immunocytochemistry (ICC) and quantified by measuring the integrated fluorescence intensity in Olig2-positive cells. Each dot represents the mean of one independent culture. ***D***, Representative Western blot for Tfr in control and Sox10-Tfr^{KO} OPCs; α-tubulin and β-actin were used as internal standards. Data represent pooled results from three independent experiments. ***E***, Total iron content was examined in control and Sox10-Tfr^{KO} OPCs using a colorimetric iron assay. Each dot represents the mean of one independent sample. Values are expressed as percentage of controls ± SEM. ***$p < 0.001$. ***F***, ***G***, Two days after mitogen withdrawal, control and Sox10-Tfr^{KO} OPCs were stained with antibodies against Olig2/Tfr, Olig2/NG2, Olig2/Olig1, Olig2/Ki67, Olig2/CC1, Olig2/CNP, and Olig2/MOG; and the percentage of double-positive cells in each experimental condition was examined by confocal microscopy. Scale bar, 80 μm. Dots represent the value of independent measures. Data represent pooled results from at least three independent cultures. Values are mean ± SEM. **$p < 0.01$. ***$p < 0.001$. ***H***, Morphologic complexity of MOG-positive cells was scored in four categories. Dots represent the value of independent measures. Data represent pooled results from at least three independent cultures. Values are mean ± SEM. **$p < 0.01$. ***$p < 0.001$.

number of Olig2-positive cells with a significant decrease in the density of mature CC1-expressing oligodendrocytes (Fig. 6*A*,*B*). Importantly, these changes caused a decline in the fraction of Olig2/CC1 double-positive cells (Fig. 6*A*,*B*). Moreover, the mitotic marker Ki67 in combination with Olig2 was used to assess OPC proliferation, and the proportion of newly generated oligodendrocytes was analyzed combining Olig2 with the immature glial marker Sox2 (S. Zhang et al., 2018) (Fig. 6*C*,*D*). A

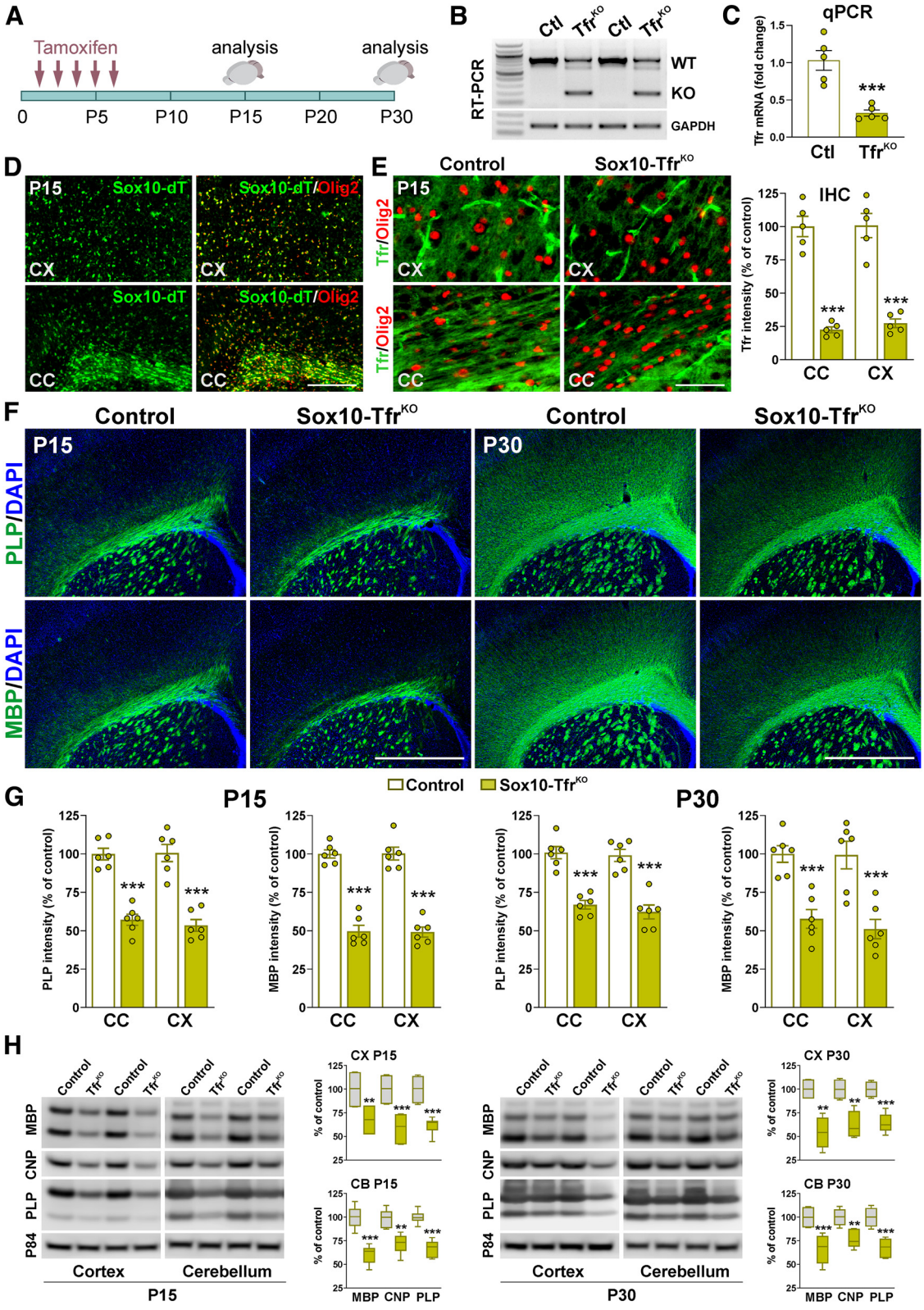

Figure 2. Myelination in the postnatal Sox10-Tfr^{KO} brain. ***A***, P2 Sox10-Tfr^{KO} and control littermates received five consecutive tamoxifen injections, and brain tissue was collected at P15 and P30. ***B***, Representative RT-PCR experiment for Tfr in cortical OPCs isolated from Sox10-Tfr^{KO} brains at P15. ***C***, qPCR for Tfr was performed in cortical OPCs isolated from Sox10-Tfr^{KO} brains at P15. Five independent samples per condition were analyzed, and Tfr mRNA was normalized to GAPDH and TBP. Values are expressed as fold change of control values ± SEM. ***$p < 0.001$ versus controls. Each dot represents the mean of one independent sample. ***D***, Olig2 immunostaining in the cortex (CX) and corpus callosum (CC) of Sox10-dTomato mice at P15. Scale bar, 90 μm. ***E***, Tfr immunostaining in the cortex and corpus callosum of Sox10-Tfr^{KO} mice at P15. Scale bar, 30 μm. Tfr expression was analyzed by measuring the integrated fluorescence intensity in the soma of Olig2-positive cells. Each dot represents the mean of one independent brain. Values are expressed as percent of control values ± SEM. ***$p < 0.001$ versus controls. ***F***, PLP and MBP immunostaining in the brain of control and Sox10-Tfr^{KO} mice at P15 and P30. Scale bar, 180 μm. ***G***, PLP and MBP expression was quantified by analyzing the integrated fluorescence intensity in the central corpus callosum (CC) and cortex (CX). Data represent pooled results from at least six brains per experimental group. Values are expressed as percentage of control values

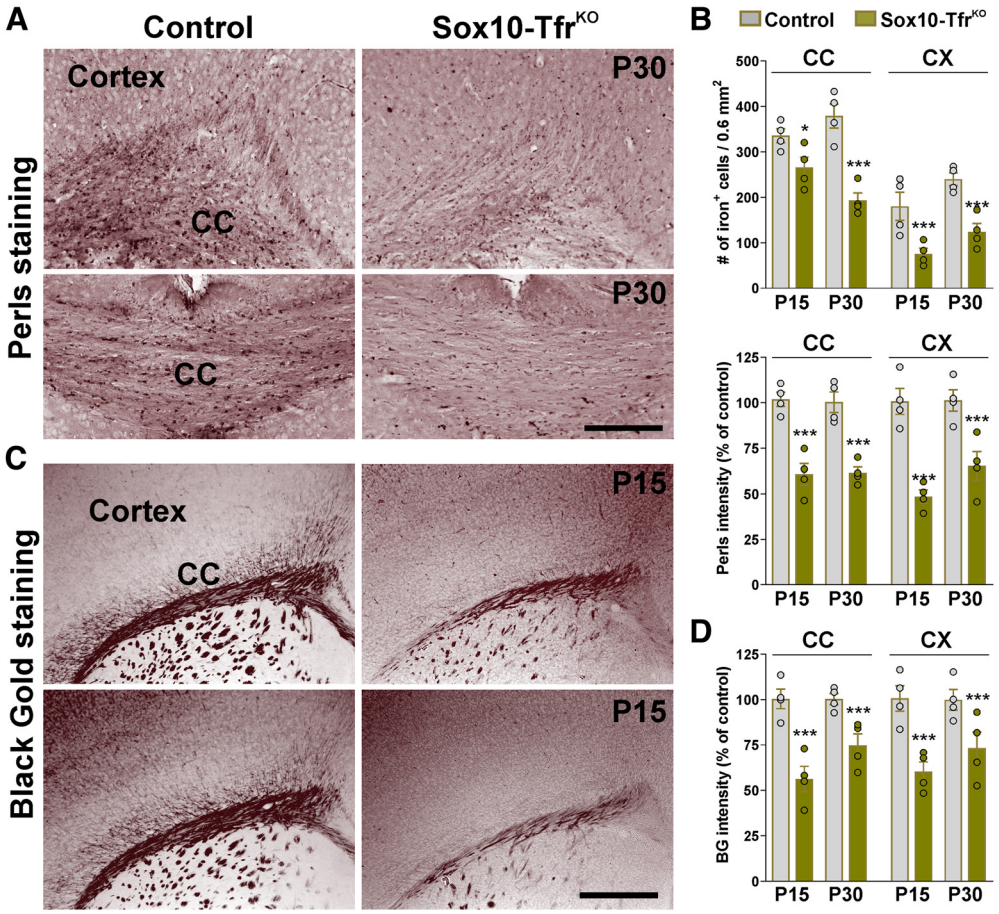

Figure 3. Perls' and Black Gold staining in the Sox10-Tfr^{KO} brain. ***A***, Perls' staining in representative brain coronal sections collected from control and Sox10-Tfr^{KO} mice at P30. Scale bar, 90 μm. ***B***, The total number of Perls' positive oligodendrocytes, and the average intensity staining per cell was quantified in the central area of the corpus callosum (CC) and cortex (CX) at P15 and P30. ***C***, Black Gold II staining in representative brain coronal sections collected from control and Sox10-Tfr^{KO} mice at P15. Scale bar, 180 μm. ***D***, Black Gold II intensity staining was quantified in the central area of the corpus callosum (CC) and cortex (CX) at P15 and P30. Data represent pooled results from at least four brains per experimental group. Values are mean ± SEM. *$p < 0.05$, ***$p < 0.001$ versus respective controls. Each dot represents the mean of 1 subject.

decrease in the number of Olig2/Sox2 double-positive cells was found in the corpus callosum and cortex of Sox10-Tfr^{KO} brains at P15 and P30 (Fig. 6*C*,*D*). In contrast, the amount of proliferating OPCs (Olig2/Ki67 double-positive cells) was equal to controls at both time points (Fig. 6*D*).

Parallel experiments were done in a conditional KO mouse in which the Tfr was ablated in NG2-positive OPCs. NG2-Tfr^{KO} (Tfr$^{f/f}$, NG2-*Cre*ER$^{Cre/-}$) mice and control (*Cre*-negative littermates (Tfr$^{f/f}$, NG2-*Cre*ER$^{-/-}$) were treated with tamoxifen from P2-P6, and brain tissue was collected at P15 and P30 for analysis. Initially, the synthesis of myelin proteins was evaluated in the corpus callosum, cortex, and striatum by immunohistochemistry. Compared with controls, NG2-Tfr^{KO} mice presented a significant decrease in the fluorescent signal for MBP and PLP in all brain areas (Fig. 7*A*,*B*). Importantly, the magnitude of these reductions was equal at both time points (Fig. 7*A*,*B*). Furthermore, examination of the oligodendrocyte population reveals a substantial decrease in the density of Olig2- and CC1-expressing cells and a decline in the fraction of Olig2/CC1 double-positive cells (Fig. 7*C*,*D*).

Iron metabolism and OPC gene expression

RNA-seq analysis was performed in cortical OPCs to study how ferritin (Fth) iron storage and iron uptake via Tfr modulate the expression of genes associated with OPC development. To delete Fth or Tfr in Sox10-positive OPCs, *Cre* activity was induced by tamoxifen (P2-P6) in Fth conditional KO mice (Sox10-Fth^{KO}; Fth$^{f/f}$, Sox10-*Cre*ER$^{Cre/-}$) (Wan et al., 2020) and Tfr conditional KO mice (Sox10-Tfr^{KO}; Tfr$^{f/f}$, Sox10-*Cre*ER$^{Cre/-}$). *Cre*-negative littermates (Fth$^{f/f}$, Sox10-*Cre*ER−/−; Tfr$^{f/f}$, Sox10-*Cre*ER−/−) were used as controls. NG2-positive OPCs were isolated from dissociated brain cortices at P15 using microbeads tagged with anti-NG2 antibodies. More than 98% of the cell were viable, and all the cells were Olig2/NG2 double-positive (Fig. 8*A*). Heatmap clustering showed high correlation across samples (Fig. 8*B*,*D*). Log_2 fold changes and their corresponding p values of all genes were used to create the volcano plot (Fig. 8*C*). Approximately 58 genes were upregulated and 53 were downregulated in Sox10-Fth^{KO} OPCs compared with control cells ($p < 0.05$, ± log_2 change) (Fig. 8*C*). Gene ontology analysis of differentially expressed genes reveals upregulated and downregulated molecular functions, cellular components, and biological processes implicated in OPC

←

± SEM. ***$p < 0.001$ versus respective controls. Each dot represents the mean of 1 subject. ***H***, Total proteins were collected from the cortex and cerebellum of control and Sox10-Tfr^{KO} animals at P15 and P30. Representative Western blots for MBP, CNP, and PLP are shown. P84 was used as the internal standard, and data from four independent experiments are summarized based on the relative spot intensities and plotted as percent of controls. Values are mean ± SEM. **$p < 0.01$, ***$p < 0.001$, versus respective controls.

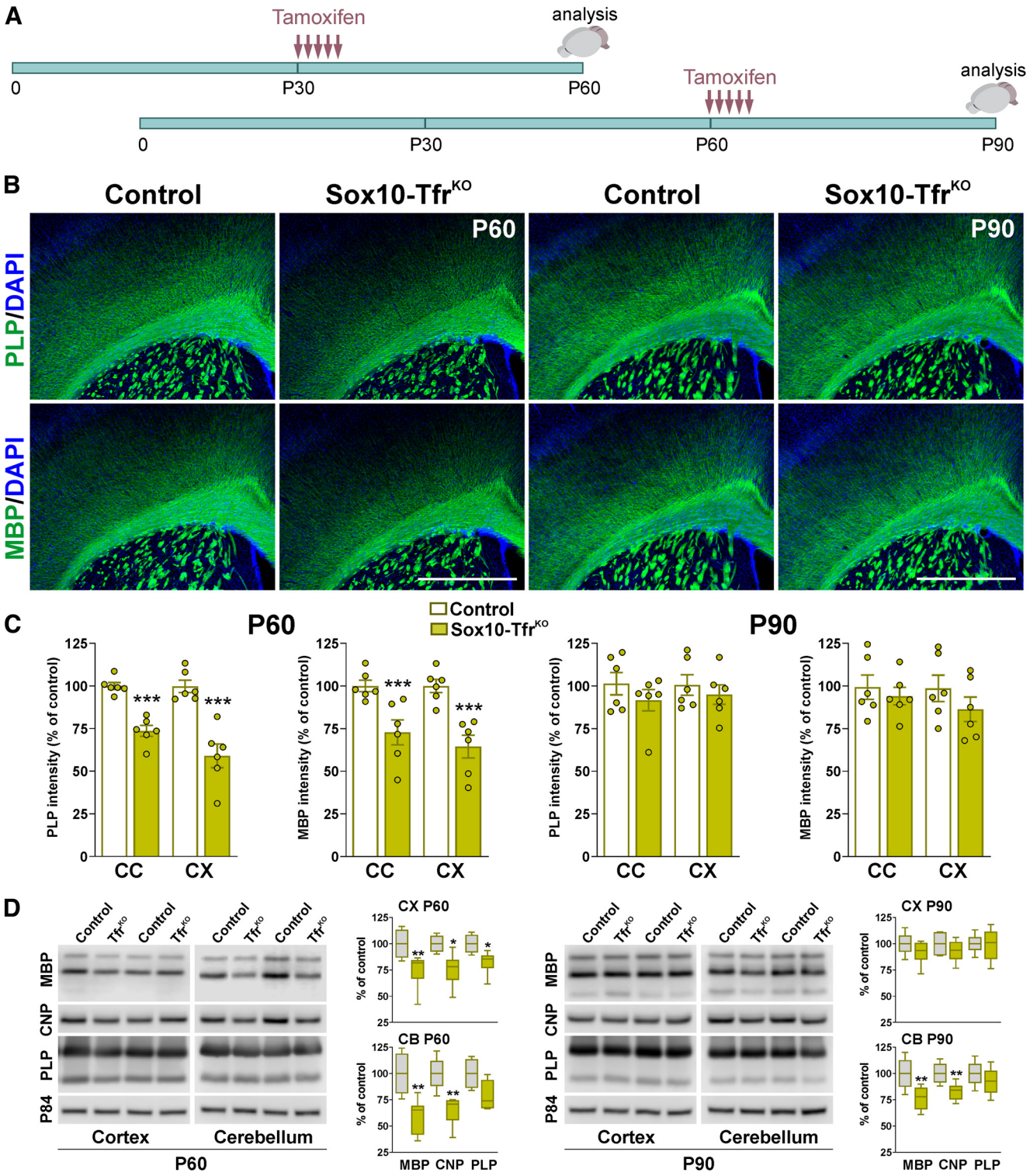

Figure 4. Myelin synthesis in adult Sox10-Tfr^{KO} mice. ***A***, P30 Sox10-Tfr^{KO} and control littermates received five consecutive tamoxifen injections, and brain tissue was collected at P60. In the second protocol, five tamoxifen injection were given to P60 Sox10-Tfr^{KO} and control animals and brain samples were collected at P90. ***B***, PLP and MBP immunostaining in the brain of control and Sox10-Tfr^{KO} mice at P60 and P90. Scale bar, 180 μm. ***C***, PLP and MBP expression was quantified by analyzing the integrated fluorescence intensity in the central corpus callosum (CC) and cortex (CX). Data represent pooled results from at least six brains per experimental group. Values are expressed as percentage of control values ± SEM. $^{***}p < 0.001$ versus respective controls. Each dot represents the mean of 1 subject. ***D***, Total proteins were collected from the cortex and cerebellum of control and Sox10-Tfr^{KO} animals at P60 and P90. Representative Western blots for MBP, CNP, and PLP are shown. P84 was used as the internal standard, and data from four independent experiments are summarized based on the relative spot intensities and plotted as percent of controls. Values are mean ± SEM. $^{*}p < 0.05$, $^{**}p < 0.01$ versus controls.

maturation, iron metabolism, and mitochondrial activity (Fig. 8*E*). GSEA of representative gene sets is shown in Figure 9. As expected, gene sets associated with oligodendrocyte development and myelination were downregulated in Sox10-Fth^{KO} OPCs (Fig. 9*A*) as well as genes implicated in OPC process extension and postsynaptic structure formation (Fig. 9*A*). In contrast, genes involved in phagocytic vesicle formation and peptidase activity were upregulated (Fig. 9*B*). Iron metabolism was also severely

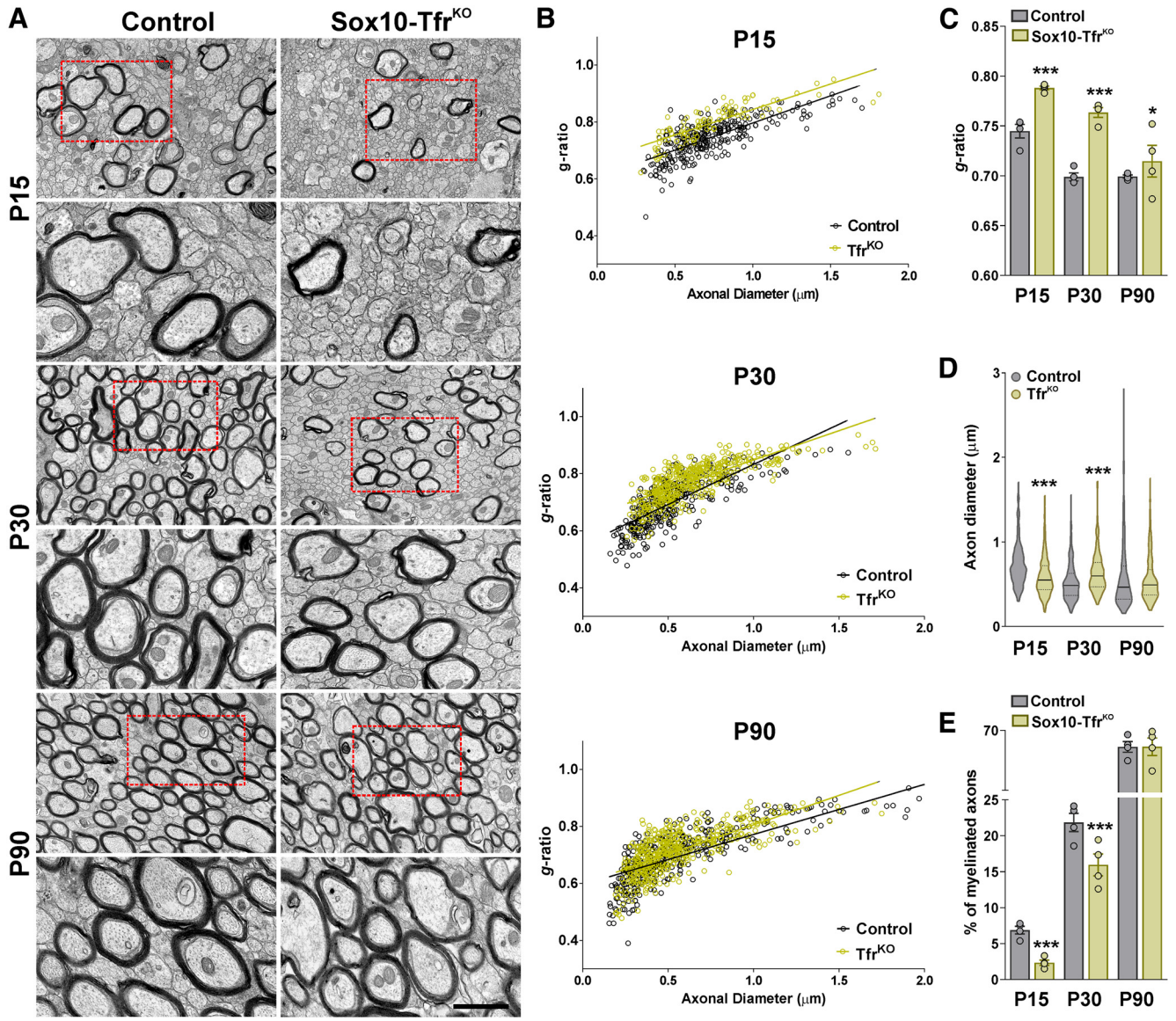

Figure 5. Electron microscopy of the Sox10-Tfr^{KO} corpus callosum. ***A***, Electron micrographs of axons in the body of the corpus callosum of control and Sox10-Tfr^{KO} mice at P15, P30, and P90. Scale bars: top, 8 μm; bottom, 2 μm. ***B***, Scatter plot of *g*-ratio values of myelinated axons. ***C***, Mean *g*-ratio values of myelinated axons for the same experimental conditions. ***D***, Mean axonal diameter of myelinated axons. ***E***, Percentage of myelinated axons. Four animals per experimental group and 200 fibers per mouse were analyzed. Values are mean ± SEM. $^{*}p < 0.05$, $^{***}p < 0.001$ versus control. ***C***, ***E***, Each dot represents the mean of 1 subject.

affected in Sox10-Fth^{KO} OPCs as GSEA analysis uncovered misregulated genes associated with iron transport, antioxidant activity, and mitochondrial activity (Fig. 9*C*,*D*). In the same line, Fth cKO OPCs display an increased activity of pro-apoptotic genes (Fig. 9*D*).

Similar analyses were performed in Sox10-Tfr^{KO} OPCs; ~134 genes were upregulated and 78 were downregulated in cells lacking the Tfr ($p < 0.05$, ± $\log_2$ change). Gene ontology evaluation in control and Sox10-Tfr^{KO} OPCs reveals upregulated and downregulated cellular components, molecular functions, and biological processes related with oligodendrocyte maturation, plasma membrane receptor activity, and mitochondrial function (Fig. 10*A*). GSEA-enrichment analysis in Sox10-Tfr^{KO} OPCs shows upregulated gene sets associated with oligodendrocyte process extension and integrin-mediated signaling (Fig. 10*C*). Additionally, Tfr deletion in cortical OPCs significantly affects the activity of the mTORC1 signaling pathway, epigenetic mechanisms critical for gene transcription and the expression of structural mitochondrial genes (Fig. 10*B*,*D*).

Discussion

Iron is usually incorporated into the cell by the Tf cycle (Moos et al., 2007). Circulating Tf binds to the Tfr in the cell plasma membrane and then undergoes endocytosis, to form an endosomal vesicle inside the cell. Previous studies have suggested that the Tfr is mainly expressed in endothelial cells of brain capillaries and neurons, but not in OPCs and/or oligodendrocytes (Roberts et al., 1993). However, our results indicate that Tfr is essential for OPC iron homeostasis and that Tfr ablation significantly affects OPC development and function. For instance, iron incorporation was decreased when Tfr was deleted in primary cultures of cortical OPCs and OPCs lacking Tfr synthesized less myelin proteins than control cells. These *in vitro* results were consistent with our *in vivo* data. We used immunohistochemical and Western blot techniques to measure the production of myelin proteins during the postnatal development of the Sox10- and NG2-Tfr^{KO} brains. Tfr^{KO} animals showed hypomyelination in several brain areas, such as the corpus callosum, cortex, and

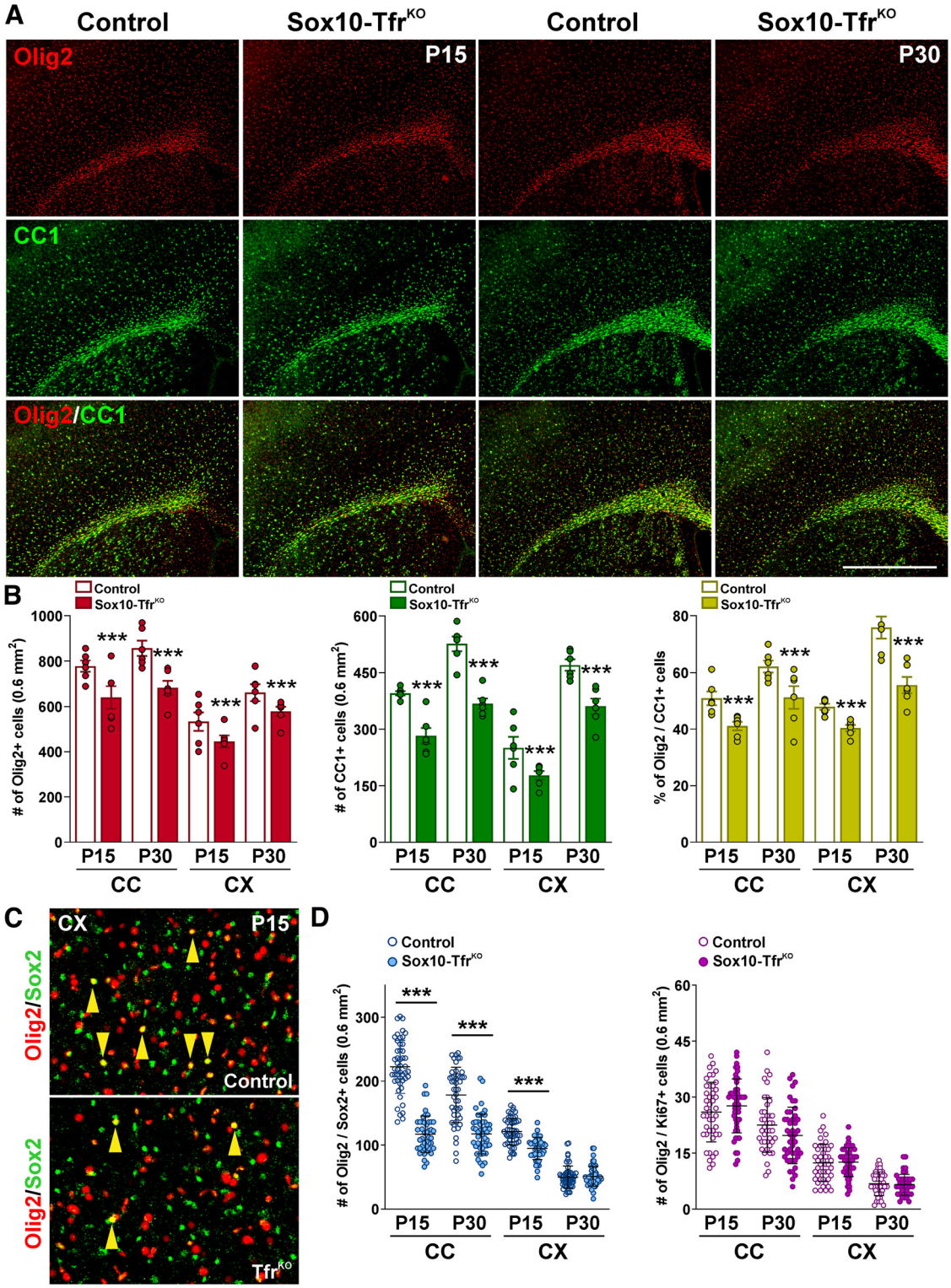

Figure 6. Decreased number of mature oligodendrocytes in the Sox10-Tfr^{KO} CNS. ***A***, Representative coronal sections from control and Sox10-Tfr^{KO} brains at P15 and P30 immunostained for Olig2 and CC1. Scale bar, 180 μm. ***B***, The total number of Olig2- and CC1-positive cells and the percentage of Olig2/CC1 double-positive cells were quantified in the central area of the corpus callosum (CC) and cortex (CX) at P15 and P30. Data represent pooled results from at least six brains per experimental group. Values are mean ± SEM. ***$p < 0.001$ versus respective controls. Each dot represents the mean of 1 subject. ***C***, Representative coronal sections from control and Sox10-Tfr^{KO} brains at P15 immunostained for Olig2 and Sox2. Scale bar, 90 μm. ***D***, The total number of Olig2/Sox2 and Olig2/Ki67 double-positive cells were quantified in the central area of the corpus callosum (CC) and cortex (CX) at P15 and P30. Data represent pooled results from at least six brains per experimental group. Scatter dot-plot graphs represent showing single brain slices values plus mean ± SD.

striatum; and the corpus callosum of Sox10-Tfr^{KO} brains displayed a substantial reduction in the percentage of myelinated axons. P15 Sox10- and NG2-Tfr^{KO} brains displayed more significant reductions in myelin protein synthesis than P30 and P60 brains, suggesting that OPCs incorporate iron via Tfr early during development. Furthermore, P90 Sox10-Tfr^{KO} mice treated with tamoxifen at P60 showed normal levels of mature oligodendrocytes and myelin, suggesting that Tfr is not essential for iron

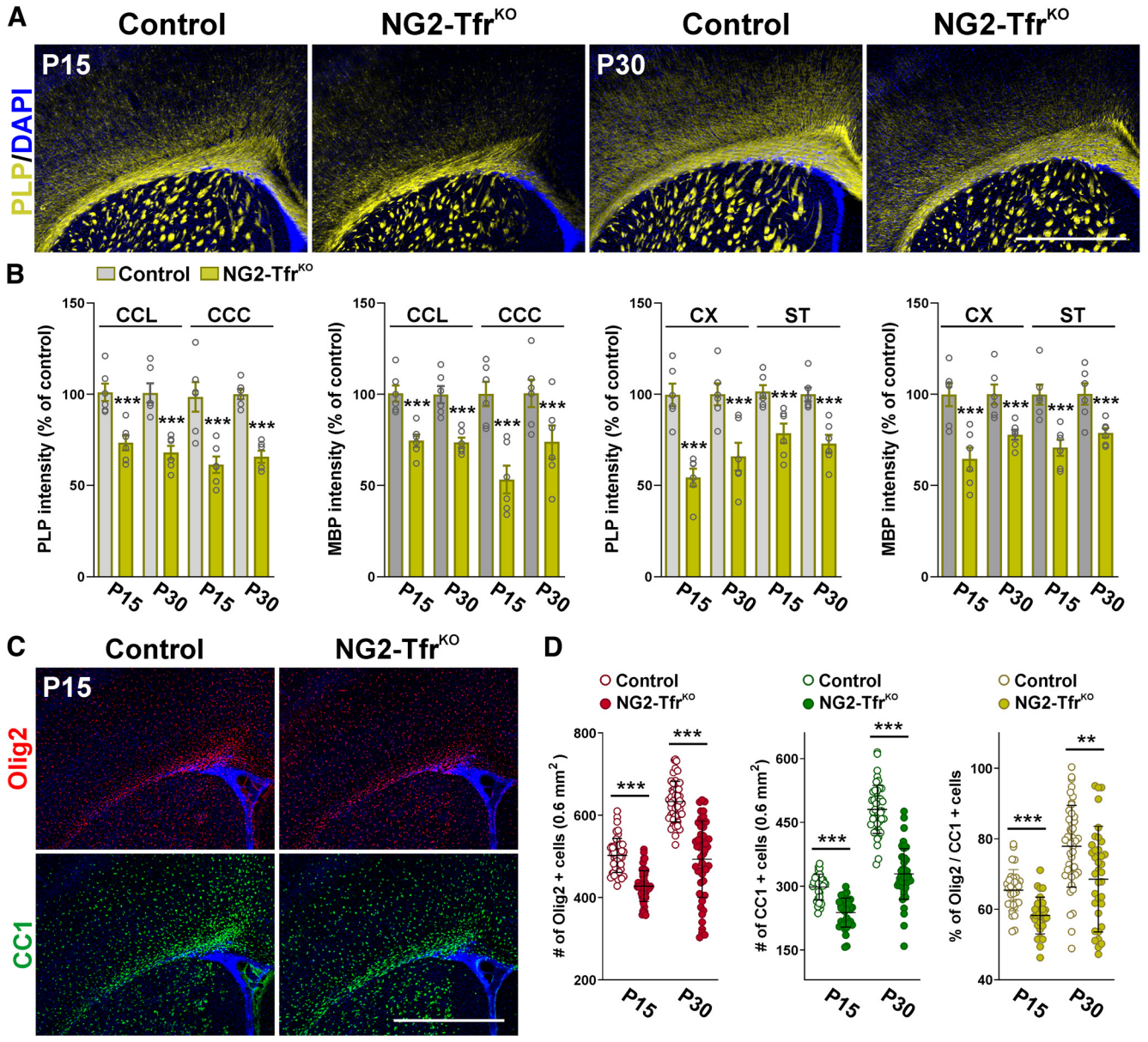

Figure 7. Myelination and oligodendrocyte numbers in the postnatal NG2-Tfr^{KO} brain. ***A***, PLP immunostaining in the brain of control and NG2-Tfr^{KO} mice at P15 and P30. Representative brain coronal sections are shown. Scale bar, 180 μm. ***B***, PLP and MBP expression was quantified by analyzing the integrated fluorescence intensity in the lateral and central corpus callosum (CCL, CCC), cortex (CX), and striatum (ST) at P15 and P30. Data represent pooled results from at least six brains per experimental group. Values are expressed as percentage of control values ± SEM. ***$p < 0.001$ versus respective controls. Each dot represents the mean of 1 subject. ***C***, Representative coronal sections from control and NG2-Tfr^{KO} brains at P15 immunostained for Olig2 and CC1. Scale bar, 180 μm. ***D***, The total number of Olig2- and CC1-positive cells and the percentage of Olig2/CC1 double-positive cells were quantified in the cortex (CX) at P15 and P30. Data represent pooled results from at least six brains per experimental group. Scatter dot-plot graphs represent showing single brain slices values plus mean ± SD.

incorporation and myelin maintenance in mature myelinating oligodendrocytes. However, we observed a slight, but significant, decrease in MBP and CNP protein expression in the cerebellum of P90 Tfr cKO mice. Thus, it is possible that, after a more prolonged period following Tfr gene inactivation, mature oligodendrocytes would display myelin synthesis abnormalities.

While it is generally accepted that iron is a requisite for myelin synthesis, it is unclear whether iron deficiency leads to global brain hypomyelination by reducing oligodendrocyte numbers, their differentiation state, or both (Todorich et al., 2009). Tfr^{KO} mice exhibited a significant decrease in the number of mature myelinating oligodendrocytes (CC1-positive cells) in combination with a reduction in the total amount of oligodendrocytes (Olig2-positive cells). Suggesting that Tfr expression is important for OPC maturation, the proportion of Olig2/CC1 double-positive cells was also decreased in these mice. Although the proliferation of Tfr cKO OPCs was found to be normal, the density of Sox2-positive OPCs was below control levels in both the corpus callosum and cortex of Tfr^{KO} brains. Together, these results indicate that Tfr is relevant for normal oligodendrocyte maturation, as well as for the survival of postnatal OPCs.

Oligodendrocytes are the most metabolically active cells in the brain and therefore require a high supply of ATP. Iron is required as a cofactor for the mitochondria oxidative chain and hence is an essential element for normal mitochondria activity and ATP production (Glinka et al., 1999; Morath and Mayer-Proschel, 2001). During development, OPCs and premyelinating oligodendrocytes have a large network of tubular mitochondria that is important for differentiation and myelin production

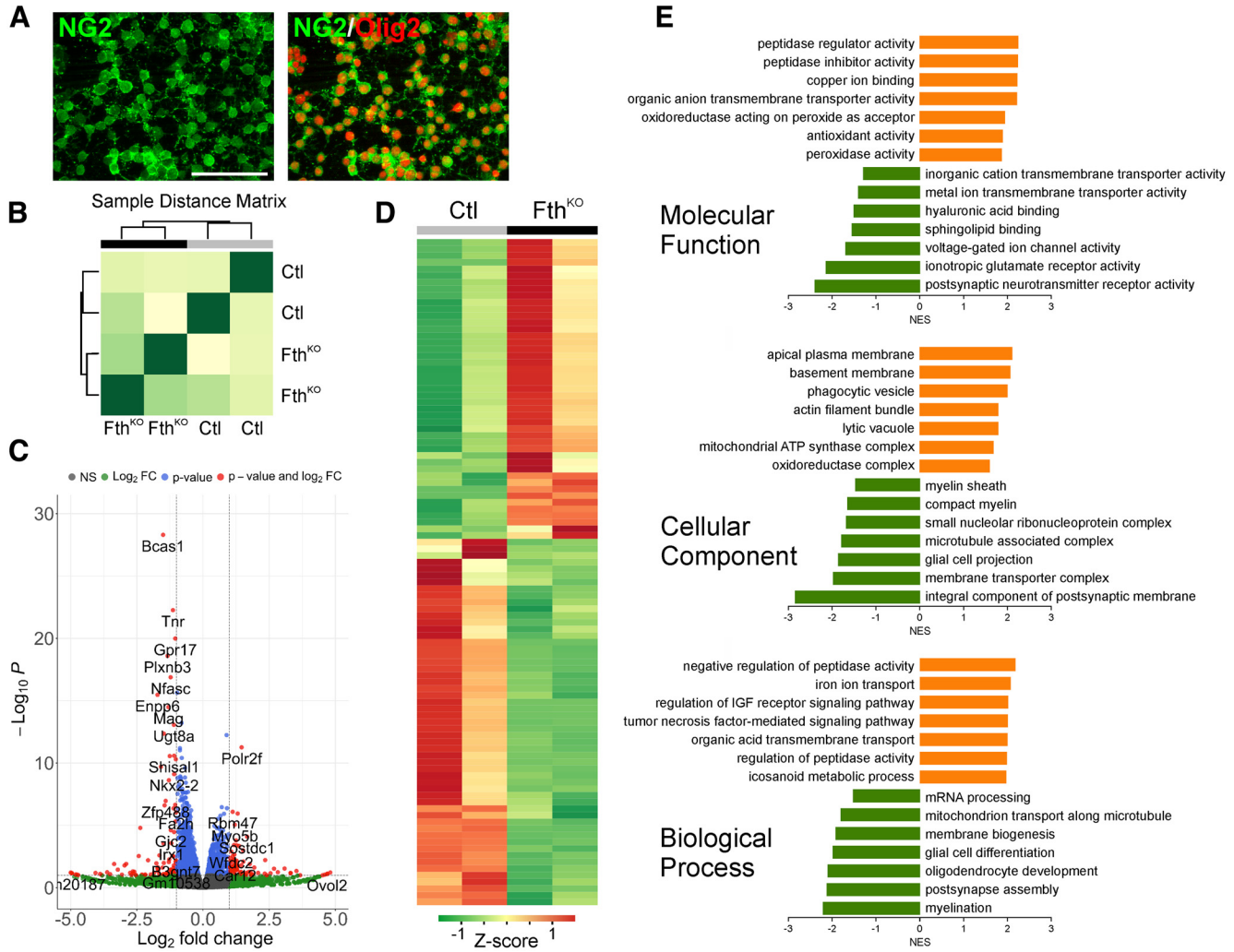

Figure 8. Transcriptomic analysis in Sox10-Fth^{KO} OPCs. ***A***, RNA-seq was done on NG2-positive OPCs purified from dissociated Sox10-Fth^{KO} brain cortices at P15. Acute isolated OPCs were stained with antibodies against NG2 and Olig2, and the percentage of double-positive cells was examined by confocal microscopy. Scale bar, 60 μm. ***B***, Heat map depicting hierarchical clustering of sample-to-sample distance. ***C***, Volcano plot map of all the genes. Differential expressed genes (DEGs) were determined while fold-change (FC) $>$ 2 and p value $<$ 0.05; 111 DEGs were found (red dot), among which 58 were upregulated (right) and 53 were downregulated (left). ***D***, A hierarchically clustered heat map showing the expression of the 100 most extreme differentially expressed genes. Red and green reprint upregulated and downregulated expression in P15 Sox10-Fth^{KO} OPCs compared with control cells. ***E***, Gene ontology (GO) term enrichment analysis for differentially expressed genes was performed using the ClusterProfiler package. The plot of GO annotation enrichment analysis for Molecular Function, Cellular Component, and Biological Processes is shown. The normalized enrichment score (NES) in the *x* axis is the relative abundance of genes in such term.

(Meyer and Rinholm, 2021). After myelination is complete, mature oligodendrocytes have fewer and more fragmented mitochondria (Meyer and Rinholm, 2021). Our transcriptome experiments show that the morphogenesis of new mitochondria is abnormal in Tfr cKO OPCs. Several genes for mitochondrial proteins, ribosomes, and respiratory chain components were downregulated in OPCs lacking Tfr. Additionally, Tfr deletion in cortical OPCs significantly affects the activity of the mammalian target of rapamycin (mTOR) signaling pathway. mTOR signaling is known to directly modulate mitochondrial dynamics and glycolysis in several cell types (Morita et al., 2013; Salmond, 2018; Xiaoyu et al., 2018; Rosario et al., 2019). Furthermore, mTOR signaling in oligodendrocytes is critical for proper CNS myelination (Lebrun-Julien et al., 2014; Wahl et al., 2014) and mTOR inhibition in differentiating OPCs results in impaired mitochondrial oxidative phosphorylation and glycolysis (Jeffries et al., 2021). Thus, the combination of mitochondrial abnormalities and alterations in the mTOR signaling pathway suggest that energy production in Tfr cKO OPCs is likely disrupted to an extent that prevents OPC maturation and myelin production, a highly energy-demanding process.

Tfr can activate intracellular signaling cascades independent of its role on iron uptake (Chen et al., 2015). For instance, Tfr internalization promotes F3-contactin and β-tubulin synthesis in OPCs, a process mediated by the activation of the Fyn kinase, MEK/ERK, and PI3K/Akt signaling pathways (Pérez et al., 2013). We found that the absence of Tfr in OPCs upregulates genes associated with the extension of processes and integrin signaling cascades. Integrin-mediated signaling is crucial to the proliferation, survival, and maturation of OPCs through the activation of downstream signaling pathways involved in cytoskeletal remodeling (O'Meara et al., 2011). The effect of integrins on OPC development is thought to be governed by extracellular matrix (ECM) components in axonal tracts (Colognato et al., 2002). Disruption of ECM-integrin connection results in a variety of developmental defects, including aberrant process and myelin sheet formation, along with delayed expression of myelin proteins. Conversely, integrin ligation facilitates the normal development

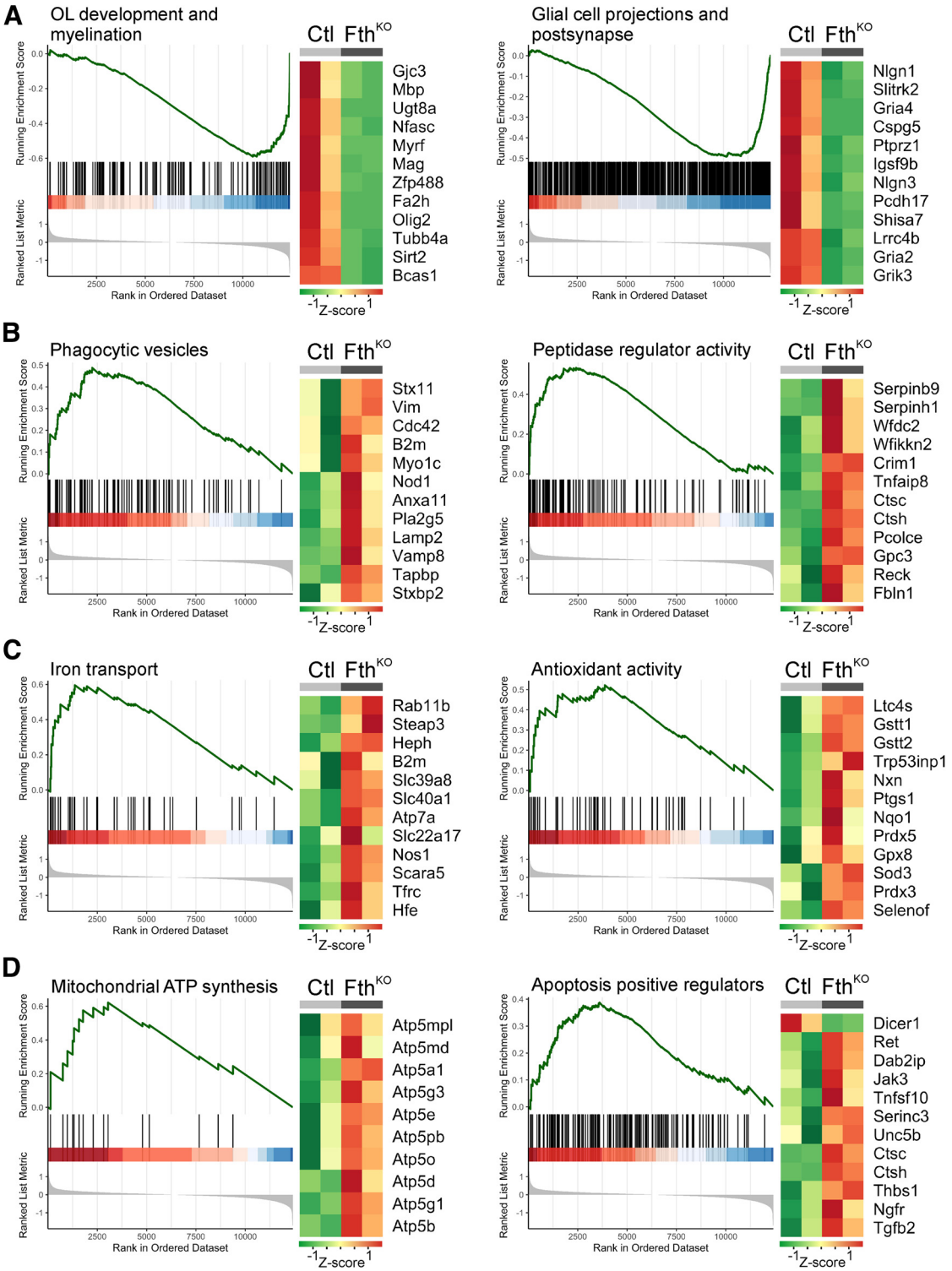

Figure 9. GSEA in Sox10-Fth^{KO} OPCs. ***A***, GSEA analysis reveals a significant inhibition of gene sets associated with oligodendrocyte development/myelination and glial cell projections/postsynapse in Sox10-Fth^{KO} OPCs. ***B***, Gene sets associated with phagocytic vesicles and peptidase activity were upregulated in Sox10-Fth^{KO} OPCs. ***C***, ***D***, Genes associated with iron transport, antioxidant activity, mitochondria ATP synthesis, and apoptosis-positive regulators were upregulated in Sox10-Fth^{KO} cells. On the *x* axis of each plot, genes are ranked from the most upregulated (left end) to the most downregulated (right end). Black vertical lines indicate the position of the genes from the biological pathway. *y* axis indicates a running enrichment score (ES), which goes up when genes are encountered in the pathway and goes down otherwise, leading to an assessment of the distribution within the set of all genes. The normalized enrichment score (NES) is inferred from permutations of the gene set and the false discovery rate (FDR). Right, Heat map represents the relative level of gene expression in the leading-edge subset, corresponding to the 12 most significant genes. Relative transcription values are color-coded from red (high) through yellow (intermediate) to green (low).

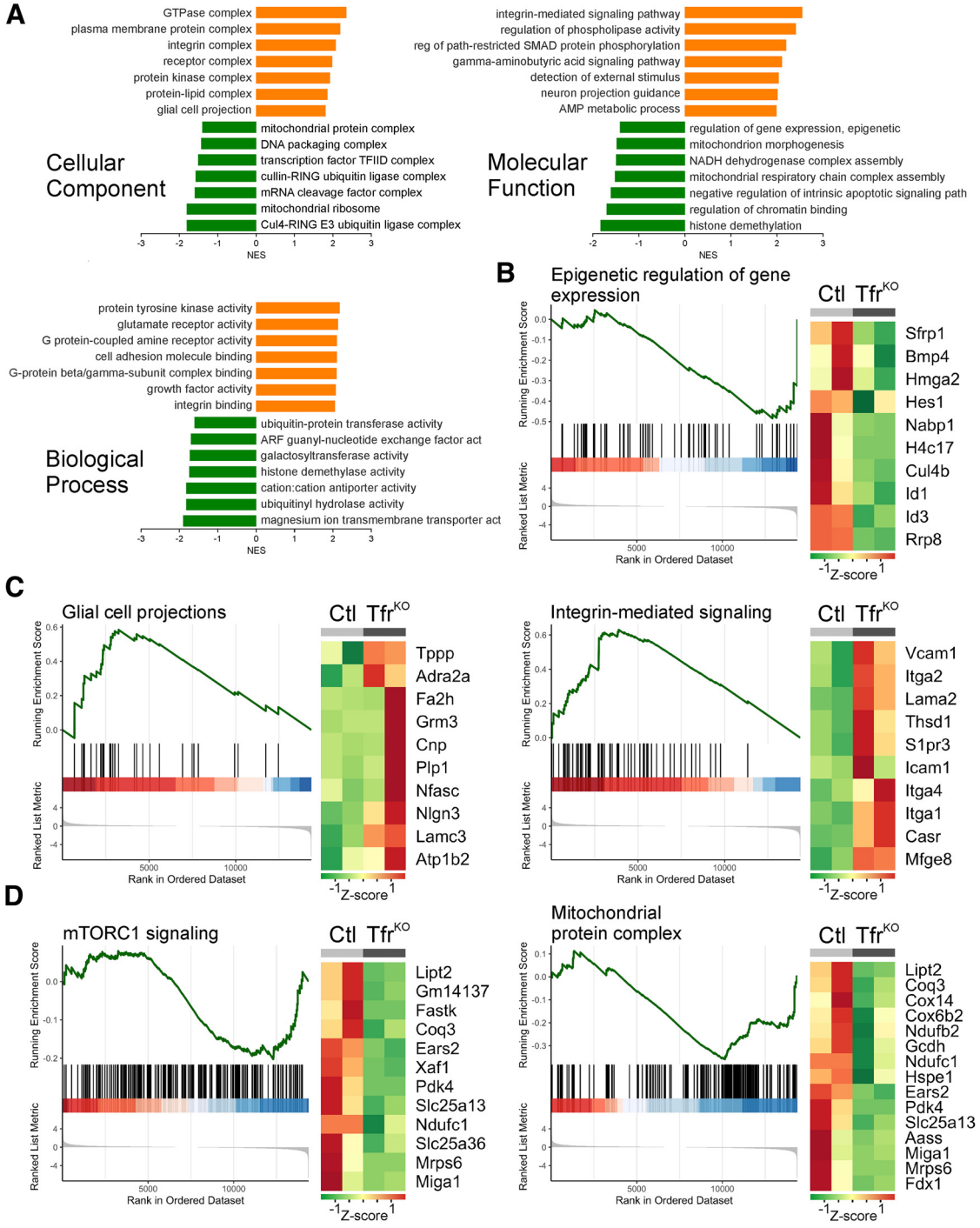

Figure 10. Transcriptomic analysis of Sox10-Tfr^{KO} OPCs. ***A***, RNA-seq was done on NG2-positive OPCs purified from dissociated Sox10-Tfr^{KO} brain cortices at P15. Gene ontology (GO) term enrichment analysis for differentially expressed genes was performed using the ClusterProfiler package. The plot of GO annotation enrichment analysis for Cellular Component, Molecular Function, and Biological Processes is shown. The normalized enrichment score (NES) in the *x* axis is the relative abundance of genes in such term. ***B***, GSEA of Sox10-Tfr^{KO} versus control cells. Gene sets associated with epigenetic regulation of gene expression were downregulated in Sox10-Tfr^{KO} OPCs. ***C***, GSEA analysis reveals activation of genes associated with glial cell projections and integrin-mediated signaling in Sox10-Tfr^{KO} OPCs. ***D***, Gene sets associated with the mTORC1 signaling pathway and mitochondrial protein complex were downregulated in Sox10-Tfr^{KO} OPCs. On the *x* axis of each plot, genes are ranked from the most upregulated (left end) to the most downregulated (right end). Black vertical lines indicate the position of the genes from the biological pathway. *y* axis indicates a running enrichment score (ES), which goes up when genes are encountered in the pathway and goes down otherwise, leading to an assessment of the distribution within the set of all genes. The normalized enrichment score (NES) is inferred from permutations of the gene set and the false discovery rate (FDR). The heat map on the right shows the relative level of gene expression in the leading-edge subset, corresponding to the 12 most significant genes. Relative transcription values are color-coded from red (high) through yellow (intermediate) to green (low).

of oligodendrocytes, as illustrated by work showing that oligodendroglial membranes are enhanced on constitutive integrin activation (Olsen and ffrench-Constant, 2005). It is likely that Tfr-deficient OPCs are increasing ECM-integrin connections to interact with axons and initiate the myelination process. However, because of their insufficient mitochondrial activity and energy production, these interactions are ineffective.

Ferritin is the main intracellular iron-storage protein and is crucial for keeping iron in a nontoxic form (Arosio et al., 2009; Y. Zhang et al., 2010). We have shown that Fth synthesis in Sox10 or NG2-positive OPCs during the first three postnatal weeks is important for OPC maturation and that Fth iron storage in adult OPCs is essential for an effective remyelination of the mouse brain (Wan et al., 2020). In this work, our RNA-seq analysis indicates that genes associated with oligodendrocyte development and myelination are downregulated in Fth^{KO} OPCs, as well as genes implicated in OPC process extension and postsynaptic structure formation. In contrast, genes involved in phagocytic vesicle formation and peptidase activity are upregulated. Together, these results indicate that the morphologic maturation of Fth cKO OPCs is compromised and that these cells are unable to extend processes normally to make proper connections with axons. Additionally, the upregulation of phagocytic vesicle formation and peptidase activity suggest that processes, and likely myelin sheaths, are being retracted and degraded. Fth cKO OPCs also display a reduction in the expression of genes implicated in mRNA processing and an increase in the activity of pro-apoptotic genes, which suggests that Fth ablation is inducing oligodendrocyte apoptotic cell death.

Iron metabolism was also significantly affected in Fth cKO OPCs. We found misregulated genes associated with iron transport, antioxidant activity, and mitochondrial function. As a result of its ability to sequester iron, Fth is considered an antioxidant protein (Balla et al., 2007). For instance, Fth production in mature oligodendrocytes is essential for an effective brain antioxidant system. It has been recently established that Fth secreted by myelinating oligodendrocytes protects axons against iron-mediated injury in the adult brain (Mukherjee et al., 2020). Antioxidant enzymes, such as the glutathione peroxidase, the superoxide dismutase, and the stress-induced heme oxygenase-1, were found to be upregulated in Fth cKO oligodendrocytes (Wan et al., 2020). In the same line, our RNA-seq analysis in Sox10-Fth^{KO} OPCs shows upregulated enzymes that play a critical role in cell redox homeostasis and oxidative stress. For example, the NAD(P)H quinone dehydrogenase (Nqo1), the peroxiredoxin (Prdx5) and nucleoredoxin (Nxn) enzymes, and the glutathione S-transferase 1 and 2 (Gsta1, 2) were among the most extreme upregulated genes in Sox10-Fth^{KO} OPCs. Thus, in the absence of Fth, oligodendrocytes may experience an increase in free cytoplasmic iron, reactive oxygen species formation, oxidative stress, and mitochondrial disfunction. These metabolic changes are likely blocking OPC maturation and inducing apoptotic cell death.

Tfr and Fth cKO OPCs showed similar reductions in intracellular iron levels (Wan et al., 2020); however, according to our transcriptomic analysis, OPCs lacking Fth displayed iron toxicity and oxidative stress which were not found in Tfr-deficient cells. This is probably the main reason behind the more severe phenotype developed by Fth cKO mice during postnatal myelination (Wan et al., 2020). However, dissimilar recombination frequencies between the Tfr locus and the Fth locus might contribute to the differences in severity of the two cKO lines. Our *in vivo* recombination experiments indicate that probably a small group of oligodendrocytes in the Tfr cKO brain express control levels of Tfr. The proliferation and maturation of these normal cells can eventually compensate the deficiencies of KO OPCs and ameliorate the hypomyelination of the Tfr cKO brain. In summary, we have established that iron uptake via Tfr and Fth iron storage are indispensable for OPC maturation and myelination. Since brain iron metabolism is disrupted in demyelinating and neurodegenerative disorders, understanding the mechanisms of iron incorporation and management in both OPCs and oligodendrocytes is an essential prerequisite for developing effective therapies for these debilitating conditions.

References

Adamo AM, Paez PM, Escobar Cabrera OE, Wolfson M, Franco PG, Pasquini JM, Soto EF (2006) Remyelination after cuprizone-induced demyelination in the rat is stimulated by apotransferrin. Exp Neurol 198:519–529.

Arosio P, Ingrassia R, Cavadini P (2009) Ferritins: a family of molecules for iron storage, antioxidation and more. Biochim Biophys Acta 1790:589–599.

Balla J, Vercellotti GM, Jeney V, Yachie A, Varga Z, Jacob HS, Eaton JW, Balla G (2007) Heme, heme oxygenase, and ferritin: how the vascular endothelium survives (and dies) in an iron-rich environment. Antioxid Redox Signal 9:2119–2137.

Beard JL, Wiesinger JA, Connor JR (2003) Pre- and postweaning iron deficiency alters myelination in Sprague-Dawley rats. Dev Neurosci 25:308–315.

Bin JM, Harris SN, Kennedy TE (2016) The oligodendrocyte-specific antibody CC1 binds Quaking 7. J Neurochem 139:181–186.

Bloch B, Popovici T, Levin MJ, Tuil D, Kahn A (1985) Transferrin gene expression visualized in oligodendrocytes of the rat brain by using in situ hybridization and immunohistochemistry. Proc Natl Acad Sci USA 82:6706–6710.

Burdo JR, Martin J, Menzies SL, Dolan KG, Romano MA, Fletcher RJ, Garrick MD, Garrick LM, Connor JR (1999) Cellular distribution of iron in the brain of the Belgrade rat. Neuroscience 93:1189–1196.

Carlson ES, Tkac I, Magid R, O'Connor MB, Andrews NC, Schallert T, Gunshin H, Georgieff MK, Petryk A (2009) Iron is essential for neuron development and memory function in mouse hippocampus. J Nutr 139:672–679.

Cheli VT, Santiago González DA, Spreuer V, Paez PM (2015) Voltage-gated Ca^{++} entry promotes oligodendrocyte progenitor cells maturation and myelination in vitro. Exp Neurol 265:69–83.

Cheli VT, Santiago González DA, Namgyal Lama T, Spreuer V, Handley V, Murphy GG, Paez PM (2016) Conditional deletion of the L-type calcium channel Cav1.2 in oligodendrocyte progenitor cells affects postnatal myelination in mice. J Neurosci 36:10853–10869.

Cheli VT, Santigo Gonzalez DA, Marziali LN, Zamora NN, Guitart ME, Spreuer V, Pasquini JM, Paez PM (2018) The divalent metal transporter 1 (DMT1) is required for iron uptake and normal development of oligodendrocyte progenitor cells. J Neurosci 38:9142–9159.

Chen AC, Donovan A, Ned-Sykes R, Andrews NC (2015) Noncanonical role of transferrin receptor 1 is essential for intestinal homeostasis. Proc Natl Acad Sci USA 112:11714–11719.

Colognato H, Baron W, Avellana-Adalid V, Relvas JB, Baron-Van Evercooren A, Georges-Labouesse E, ffrench-Constant C (2002) CNS integrins switch growth factor signaling to promote target-dependent survival. Nat Cell Biol 4:833–841.

Connor JR, Menzies SL (1996) Relationship of iron to oligodendrocytes and myelination. Glia 17:83–93.

Darshan D, Vanoaica L, Richman L, Beermann F, Kühn LC (2009) Conditional deletion of ferritin H in mice induces loss of iron storage and liver damage. Hepatology 50:852–860.

Dobin A, Davis CA, Schlesinger F, Drenkow J, Zaleski C, Jha S, Batut P, Chaisson M, Gingeras TR (2013) STAR: ultrafast universal RNA-seq aligner. Bioinformatics 29:15–21.

Escobar-Cabrera OE, Zakin MM, Soto EF, Pasquini JM (1997) Single intracranial injection of apotransferrin in young rats increases the expression of specific myelin protein mRNA. J Neurosci Res 47:603–608.

Espinosa de los Monteros A, Sawaya BE, Guillou F, Zakin MM, de Vellis J, Schaeffer E (1994) Brain-specific expression of the human transferrin gene: similar elements govern transcription in oligodendrocytes and in a neuronal cell line. J Biol Chem 269:24504–24510.

Franklin KB, Paxinos G (2008) The mouse brain in stereotaxic coordinates. San Diego: Academic.

Glinka Y, Gassen M, Youdim MB, Connor JR (1999) Iron and neuro-transmitter function in the brain. In: Metals and oxidative damage in neurological disorders, pp 1–22. Springer:New York, NY.

Guardia-Clausi M, Paez PM, Campagnoni AT, Pasquini LA, Pasquini JM (2012) Intranasal administration of aTf protects and repairs the neonatal white matter after a cerebral hypoxic-ischemic event. Glia 60:1540–1554.

Gunshin H, Fujiwara Y, Custodio AO, Direnzo C, Robine S, Andrews NC (2005) Slc11a2 is required for intestinal iron absorption and erythropoiesis but dispensable in placenta and liver. J Clin Invest 115:1258–1266.

Jeffries MA, McLane LE, Khandker L, Mather ML, Evangelou AG, Kantak D, Bourne JN, Macklin WB, Wood TL (2021) mTOR signaling regulates metabolic function in oligodendrocyte precursor cells and promotes efficient brain remyelination in the cuprizone model. J Neurosci 41:8321–8337.

Lebrun-Julien F, Bachmann L, Norrmén C, Trötzmüller M, Köfeler H, Rüegg MA, Hall MN, Suter U (2014) Balanced mTORC1 activity in oligodendrocytes is required for accurate CNS myelination. J Neurosci 34:8432–8448.

Li Y, Guan Q, Chen Y, Han H, Liu W, Nie Z (2013) Transferrin receptor and ferritin-H are developmentally regulated in oligodendrocyte lineage cells. Neural Regen Res 8:6–12.

Liao Y, Smyth GK, Shi W (2014) featureCounts: an efficient general-purpose program for assigning sequence reads to genomic features. Bioinformatics 30:923–930.

Love MI, Huber W, Anders S (2014) Moderated estimation of fold change and dispersion for RNA-seq data with DESeq2. Genome Biol 15:550.

Matsuoka T, Ahlberg PE, Kessaris N, Iannarelli P, Dennehy U, Richardson WD, McMahon AP, Koentges G (2005) Neural crest origins of the neck and shoulder. Nature 436:347–355.

Meijer DH, Kane MF, Mehta S, Liu H, Harrington E, Taylor CM, Stiles CD, Rowitch DH (2012) Separated at birth? The functional and molecular divergence of Olig1 and Olig2. Nat Rev Neurosci 13:819–831.

Meyer N, Rinholm JE (2021) Mitochondria in myelinating oligodendrocytes: slow and out of breath? Metabolites 11:359.

Moos T, Rosengren Nielsen T, Skjørringe T, Morgan EH (2007) Iron trafficking inside the brain. J Neurochem 103:1730–1740.

Morath DJ, Mayer-Proschel M (2001) Iron modulates the differentiation of a distinct population of glial precursor cells into oligodendrocytes. Dev Biol 237:232–243.

Morita M, Gravel SP, Chenard V, Sikstrom K, Zheng L, Alain T, Gandin V, Avizonis D, Arguello M, Zakaria C, McLaughlan S, Nouet Y, Pause A, Pollak M, Gottlieb E, Larsson O, St-Pierre J, Topisirovic I, Sonenberg N (2013) mTORC1 controls mitochondrial activity and biogenesis through 4E-BP-dependent translational regulation. Cell Metab 18:698–711.

Mukherjee C, Kling T, Russo B, Miebach K, Kess E, Schifferer M, Pedro LD, Weikert U, Fard MK, Kannaiyan N, Rossner M, Aicher ML, Goebbels S, Nave KA, Krämer-Albers EM, Schneider A, Simons M (2020) Oligodendrocytes provide antioxidant defense function for neurons by secreting ferritin heavy chain. Cell Metab 32:259–272.e10.

O'Meara RW, Michalski JP, Kothary R (2011) Integrin signaling in oligodendrocytes and its importance in CNS myelination. J Signal Transduct 2011:354091.

Olsen IM, ffrench-Constant C (2005) Dynamic regulation of integrin activation by intracellular and extracellular signals controls oligodendrocyte morphology. BMC Biol 3:25.

Ortiz E, Pasquini JM, Thompson K, Felt B, Butkus G, Beard J, Connor JR (2004) Effect of manipulation of iron storage, transport, or availability on myelin composition and brain iron content in three different animal models. J Neurosci Res 77:681–689.

Paez PM, Garcia CI, Davio C, Campagnoni AT, Soto EF, Pasquini JM (2004) Apotransferrin promotes the differentiation of two oligodendroglial cell lines. Glia 46:207–217.

Paez PM, Garcıa CI, Campagnoni AT, Soto EF, Pasquini JM (2005) Overexpression of human transferrin in two oligodendroglial cell lines enhances their differentiation. Glia 52:1–15.

Paez PM, Garcia CI, Pasquini JM (2006) Expression of myelin basic protein in two oligodendroglial cell lines is modulated by apotransferrin through different transcription factors. J Neurosci Res 83:606–618.

Pérez MJ, Fernandez N, Pasquini JM (2013) Oligodendrocyte differentiation and signaling after transferrin internalization: a mechanism of action. Exp Neurol 248:262–274.

Reinert A, Morawski M, Seeger J, Arendt T, Reinert T (2019) Iron concentrations in neurons and glial cells with estimates on ferritin concentrations. BMC Neurosci 20:25.

Roberts RL, Fine RE, Sandra A (1993) Receptor-mediated endocytosis of transferrin at the blood-brain barrier. J Cell Sci 104:521–532.

Roetto A, Bosio S, Gramaglia E, Barilaro MR, Zecchina G, Camaschella C (2002) Pathogenesis of hyperferritinemia cataract syndrome. Blood Cells Mol Dis 29:532–535.

Rosario FJ, Gupta MB, Myatt L, Powell TL, Glenn JP, Cox L, Jansson T (2019) Mechanistic target of rapamycin complex 1 promotes the expression of genes encoding electron transport chain proteins and stimulates oxidative phosphorylation in primary human trophoblast cells by regulating mitochondrial biogenesis. Sci Rep 9:246.

Saleh MC, Espinosa de los Monteros A, de Arriba Zerpa GA, Fontaine I, Piaud O, Djordjijevic D, Baroukh N, Garcia-Otin AL, Ortiz E, Lewis S, Fiette L, Santambrogio P, Belzung C, Connor JR, de Vellis J, Pasquini JM, Zakin MM, Baron B, Guillou F (2003) Myelination and motor coordination are increased in transferrin transgenic mice. J Neurosci Res 72:587–594.

Salmond RJ (2018) mTOR regulation of glycolytic metabolism in T cells. Front Cell Dev Biol 6:122.

Santiago González DA, Cheli VT, Zamora NN, Namgyal Lama T, Spreuer V, Murphy GG, Paez PM (2017) Conditional deletion of the L-type calcium channel Cav1.2 in NG2 positive cells delay remyelination in mice. J Neurosci 37:10038–10051.

Sperber BR, McMorris FA (2001) Fyn tyrosine kinase regulates oligodendroglial cell development but is not required for morphological differentiation of oligodendrocytes. J Neurosci Res 63:303–312.

Stephenson E, Nathoo N, Mahjoub Y, Dunn JF, Yong VW (2014) Iron in multiple sclerosis: roles in neurodegeneration and repair. Nat Rev Neurol 10:459–468.

Taylor EM, Morgan EH (1990) Developmental changes in transferrin and iron uptake by the brain in the rat. Brain Res Dev Brain Res 55:35–42.

Todorich B, Pasquini JM, Garcia CI, Paez PM, Connor JR (2009) Oligodendrocytes and myelination: the role of iron. Glia 57:467–478.

Wahl SE, McLane LE, Bercury KK, Macklin WB, Wood TL (2014) Mammalian target of rapamycin promotes oligodendrocyte differentiation, initiation, and extent of CNS myelination. J Neurosci 34:4453–4465.

Wan R, Cheli VT, Santiago González DA, Wan Q, Rosenblum SL, Paez PM (2020) Impaired postnatal myelination in a conditional knock-out mouse for the ferritin heavy chain in oligodendrocyte progenitor cells. J Neurosci 40:7609–7624.

Wu T, Hu E, Xu S, Chen M, Guo P, Dai Z, Feng T, Zhou L, Tang W, Zhan L, Fu X, Liu S, Bo X, Yu G (2021) Cluster Profiler 4.0: a universal enrichment tool for interpreting omics data. Innovation (Camb) 2:100141.

Xiaoyu H, Yiru Y, Shuisheng S, Keyan C, Zixing Y, Shanglin C, Yuan W, Dongming C, Wangliang Z, Xudong B, Jie M (2018) The mTOR pathway regulates PKM2 to affect glycolysis in esophageal squamous cell carcinoma. Technol Cancer Res Treat 17:1533033818780063.

Zamora NN, Cheli VT, Santiago González DA, Wan R, Paez PM (2020) Deletion of voltage-gated Ca^{++} channels in astrocytes during demyelination reduces brain inflammation and promotes myelin regeneration in mice. J Neurosci 40:3332–3347.

Zhang S, Zhu X, Gui X, Croteau C, Song L, Xu J, Wang A, Bannerman P, Guo F (2018) Sox2 is essential for oligodendroglial proliferation and differentiation during postnatal brain myelination and CNS remyelination. J Neurosci 38:1802–1820.

Zhang Y, Mikhael M, Xu D, Li Y, Soe-Lin S, Ning B, Li W, Nie G, Zhao Y, Ponka P (2010) Lysosomal proteolysis is the primary degradation pathway for cytosolic ferritin and cytosolic ferritin degradation is necessary for iron exit. Antioxid Redox Signal 13:999–1009.

Zhang Y, Chen K, Sloan SA, Bennett ML, Scholze AR, O'Keeffe S, Phatnani HP, Guarnieri P, Caneda C, Ruderisch N, Deng S, Liddelow SA, Zhang C, Daneman R, Maniatis T, Barres BA, Wu JQ (2014) An RNA-sequencing transcriptome and splicing database of glia, neurons, and vascular cells of the cerebral cortex. J Neurosci 34:11929–11947.

Zhu X, Hill RA, Dietrich D, Komitova M, Suzuki R, Nishiyama A (2011) Age-dependent fate and lineage restriction of single NG2 cells. Development 138:745–753.